

# Lattice gauge theory and dynamical quantum phase transitions using noisy intermediate scale quantum devices

Simon Panyella Pedersen\*

*Department of Physics and Astronomy, Aarhus University, DK-8000 Aarhus C, Denmark*

N. T. Zinner†

*Department of Physics and Astronomy, Aarhus University, DK-8000 Aarhus C, Denmark and  
Aarhus Institute of Advanced Studies, Aarhus University, DK-8000 Aarhus C, Denmark*

(Dated: October 6, 2021)

With noisy intermediate scale quantum devices in mind, we propose a class of superconducting circuits for the general implementation of  $U(1)$  lattice gauge models via the formalism of quantum link models. The circuit can be modularly scaled to any lattice configuration. Simulating the circuit dynamics with realistic circuit parameters we find that it implements the target dynamics with a steady average fidelity of 99.5% or higher. The principles of these circuits can be generalized to implement other, more complicated gauge symmetries. Finally, we consider readout of the circuit using a method that yields information about all the degrees of freedom with resonators coupled dispersively to only a subset of them. As an example of interesting physics to study with this we show how such a quantum link model on a periodic chain exhibits dynamical quantum phase transitions by studying the Loschmidt amplitude and a novel gauge invariant string order parameter. The zeros of the Loschmidt amplitude as well as the zeros of our order parameter are revealed by vortices in their phases, which can be counted by a topologically invariant winding number.

## I. INTRODUCTION

There is an increasing study of non-equilibrium quantum dynamics as improving experimental quantum control makes it accessible [1]. Quantum simulators have been realized with cold atoms in optical lattices, ions, and superconducting quantum circuits (SQCs) among others, and have already been used to study exciting dynamical phenomena like time crystals [2, 3], many-body localization [4, 5], prethermalization and thermalization [6–8], and particle-antiparticle creation and annihilation [9]. A newly emerging addition to these is dynamical quantum phase transitions (DQPTs) [10–22]. These phase transitions have been studied experimentally [23–26], and offer a broad spectrum of fascinating physics, like a connection to topology [27–30], allowing for the definition of dynamical topological order parameters [26, 31], vortex dynamics [32], scaling and universality [11], and a showing both a connection to underlying equilibrium phase transitions [10, 28, 33], as well as being completely independent of them [34–36], the latter showing their truly non-equilibrium nature. A particularly interesting type of system for the study of dynamics is gauge theories, specifically lattice gauge theories (LGTs) [37–39]. Gauge theories are at the basis of our understanding of particle physics, and are notoriously difficult to handle both analytically and numerically. They are thus ideally suited for analog simulation [40–47]. DQPTs in gauge theories have been studied numerically [17, 30], as well as analytically in the non-interacting limit in Ref. [30], but

have yet to be observed experimentally to the best of our knowledge. In this work we show how to obtain LGTs, in the form of quantum link models (QLM) [17, 40, 48–51], in SQCs in a fully consistent way, showing that we get the desired Hamiltonians with very high fidelity. We use the example of  $U(1)$  to demonstrate this, and we show that exploring the new field of DQPTs is possible with NISQ-era devices [52]. Through use of the eigenmodes of the capacitive network (also known as normal or electrical modes) [53–57] the circuit implements three spin-1/2's interacting via Z-type couplings and a direct three-body XXX-coupling. Through appropriate tuning the XXX-coupling yields the desired  $U(1)$  invariant interaction necessary for the analog simulation of a  $U(1)$  QLM. The Z-type couplings essentially just shift the energy levels of the system, and do not disturb the desired feature of the circuit, but merely make more complicated numerical tuning necessary. We find that with appropriately tuned parameters the circuit implements the desired dynamics with an average fidelity of about 99.5% or higher, with most of the loss caused by leakage to higher levels, which could be further suppressed at the cost of slower dynamics. The circuit can be scaled in a modular way to construct any desired spin lattice configuration. We then study a particular  $U(1)$  symmetric system, the massive Schwinger model [9, 30, 58, 59], exhibiting DQPTs after a quench for all system sizes considered, and we show how the smallest, non-trivial version can be realized with our SQC. Furthermore, we provide a readout scheme for how to observe this in concrete setups, inspired by that of Refs. [55, 56]. This makes it possible now to use NISQ devices to do precision studies of LGTs and DQPTs.

\* spp@phys.au.dk

† zinner@phys.au.dk

## II. RESULTS

### A. Target QLM Hamiltonian

The system we wish to realize with our circuit is the following example of an interacting LGT: the (1+1)D U(1) invariant theory of fermions on a periodic lattice interacting via an electric-like field. We represent the fermionic field with spinless, staggered mass fermions on the sites of the lattice, and transform these via the Jordan-Wigner transformation [51, 60–62] into spin-1/2's. We will be working in the quantum link model framework [17, 40, 48–51], where gauge fields, living on the links of the lattice, are represented by spin-1/2's. Thus the entire model is represented by a spin-1/2 system. The Hamiltonian for this system is

$$H = \sum_{n=0}^{N-1} \left[ -(-1)^n \frac{m}{2} \sigma_n^z + \frac{J}{2} (\sigma_n^+ S_{n,n+1}^+ \sigma_{n+1}^- + \text{H.c.}) \right] \quad (1)$$

where  $N$  is the number of matter sites, which must be even to conserve the symmetry between particles and antiparticles,  $m$  is the staggered mass of the fermions, and  $J$  is the matter-gauge coupling strength.  $\sigma_n^\alpha$  and  $S_{n,n+1}^\alpha$  with  $\alpha = z, +, -$  are Pauli-Z, step-up and -down matrices pertaining to the matter field spin at site  $n$ , and the gauge field spin on the link connecting site  $n$  and site  $n+1$ , respectively. After going through our proposal for a circuit realization of this system, we will consider quenches of the sign of the mass  $m \rightarrow -m$  and the resulting DQPTs.

### B. Circuit realization

We present a circuit that implements two matter site spins and a gauge link spin interacting via a direct three-body XXX-coupling, which through appropriate tuning yields the desired U(1) interaction seen in Eq. (1) in the rotating wave approximation (RWA). The circuit scales naturally in a modular fashion, and could be used to create large 1D chains, 2D lattices, or any other configuration of matter sites interacting through gauge links. Hence, the circuit could be used to experimentally implement dynamics in 1D or 2D models, to study for example vacuum quenches similar to what we will look at below, or strong CP-breaking in gauge models. Fig. 1c shows a diagrammatic implementation of a plaquette of four sites, hinting how a 2D configuration would have to be made. Early work was done to indicate that circuits could be used for simulating LGTs [62–71], but this work did not consider concrete cases in detail, nor any checks whether the circuits actually realize the right dynamics with high fidelity. Here we do those things for the first time. We directly compare the time evolution operator implemented by our circuit with the desired time evolution operator of the U(1) spin-1/2 QLM presented above using average fidelity [72].

The circuit can be seen in Fig. 1a. It consists of four all-to-all connected nodes, and we may divide the branches in two groups. The blue and red branches have the same circuit elements but each their own circuit parameters. They each host a transmon-like [73] anharmonic oscillator mode, implementing a spin representing a matter field. The purple branches likewise have the same circuit elements, with identical parameters, and they connect the blue and red branches to each other. These branches together host another anharmonic mode which implements a spin that then represents the gauge link. A similar circuit was designed and experimentally tested in Ref. [74] to realize a qubit with a very long life time. Each node has been coupled capacitively to ground via an identical capacitance  $K$ . Ideally this capacitance is zero, but has been included to study the effects of coupling to ground as well as capacitive coupling to control or readout devices. There are four external fluxes,  $\Phi_i$  for  $i = 1, 2, 3, 4$ , threaded through loops that each consist of two Josephson junctions in parallel, in the purple branches. The Josephson junctions themselves are imagined as implemented with SQUIDs such that the Josephson energy of each has an increased interval of possible values and high tunability. In Fig. 1b the layout of the circuit is chosen such that the  $\Phi_i$  only pass through the circuit loops with the Josephson junctions pertaining to  $E_s$ , using airbridges [75–80]. The modular scalability of the circuit has also been made explicit in this diagram. The idea is to make copies of the circuit in sequence, while using the same branches for the matter site spins. The circuit can thus be quite intuitively scaled to a chain of matter sites interacting through gauge links. A matter site branch could potentially also be shared by more than two copies of the circuit, making it possible to realize more complicated configurations. This would however result in many wires connecting to the same branch and require many bridges. The ability to cross conductors via airbridges makes SQCs a suitable platform to implement periodic boundary conditions. Bridges make it possible to access all points in a complicated circuit, while keeping it planar. In order to simulate the periodic system described by Eq. (1) for the simple case of  $N = 4$  (which we show below hosts DQPTs), we would have four copies of the circuit put together in this way, forming a square. A simple diagram of this can be seen in Fig. 1c. In the next section we will consider readout of the circuit by dispersively coupling resonators to just the matter site branches, i.e. readout of the square would be done by coupling resonators to its corner branches (the red and blue).

In the following we will consider only a single copy of the circuit, using circuit parameters optimized for that case. Putting several together to form a square or some larger system, the circuit parameters would have to be retuned. However, only the modes on the branches which are shared with the new copies will be affected by them, i.e. the matter field modes. These do, however, have their own circuit parameters, which affect only the mat-

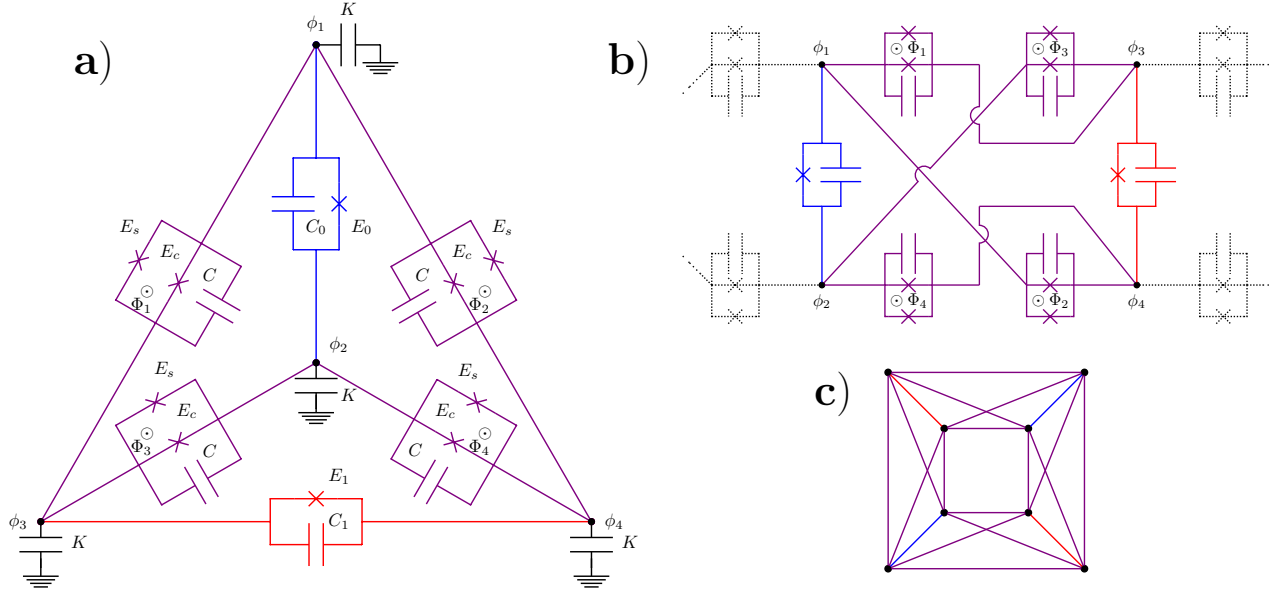


Figure 1. (a) The diagram of the circuit used to implement three spins interacting via a direct three-body XXX-coupling. Notice the identical circuit parameters. The identical grounding of each node has been included only for completeness of the study. We implement the spins via the eigenmodes of the capacitive network. The branches pertaining to each of these modes have been coloured separately. The blue and red branches will implement matter sites spins, while the purple branches implement the gauge link spin. (b) The same circuit but now folded to make the modular scalability of the circuit completely clear. Multiple copies of the circuit, sharing the matter site branches pairwise, will implement a chain of matter sites coupled via gauge links. (c) A simple diagram of how four copies of the circuit could be put together to implement the periodic  $N = 4$  version of Eq. (1).

ter modes. These are the parameters with a subscript in Fig. 1a on the red and blue branches. Hence, the effect of the new copies could be compensated for by changing these parameters correspondingly. Hence, we are assured that if there is a good set of parameters for the case of just one copy, we could easily find parameters for several copies put together. In our study we have found that it is not difficult to optimize the parameters for the circuit, and in the Supplemental Information we show an example of these that we use in the following.

Truncating the anharmonic modes to their two lowest levels, we find that this circuit implements the following Hamiltonian (see the Methods section)

$$\begin{aligned}
 H_s = & -\frac{1}{2}\Omega_0\sigma_0^z - \frac{1}{2}\Omega_g\sigma_g^z - \frac{1}{2}\Omega_1\sigma_1^z \\
 & + J_{0g}^z\sigma_0^z\sigma_g^z + J_{01}^z\sigma_0^z\sigma_1^z + J_{g1}^z\sigma_g^z\sigma_1^z \\
 & + J_{0g1}^z\sigma_0^z\sigma_g^z\sigma_1^z + J_{0g1}^x\sigma_0^x\sigma_g^x\sigma_1^x
 \end{aligned} \quad (2)$$

where the  $\Omega$ 's and  $J$ 's are spin model parameters. To calculate the parameters we use a method introduced by the authors in Ref. [81], which avoids approximating the trigonometric functions via a Taylor expansion, but instead takes their full effect into account. This gives more accurate parameters, when truncating the flux Hamiltonian, and can be used for any sine or cosine of a linear combination of the flux coordinates. The ex-

act dependence of the spin model parameters on the circuit parameters, and details on their derivation can be seen in the Supplemental Information. The circuit has thus resulted in three spins interacting through several Z-type couplings, and a direct XXX-coupling. Through appropriate tuning the XXX-coupling can be reduced to  $\sigma_0^+\sigma_g^+\sigma_1^- + \text{H.c.}$  in a RWA, which is exactly the U(1) gauge coupling in Eq. (1),  $\sigma_0^+S_{0,1}^+\sigma_1^- + \text{H.c.}$ . The main effect of the principally undesirable Z-type couplings is to shift energy levels, which we can compensate for. More importantly there are interactions between the spin-1/2 subspace and higher levels, which are similar to the Z-type couplings and have similar coupling strengths. These disturb the desired dynamics by leaking population out of the spin-1/2 subspace, and virtual interactions via these renormalize the spin model parameters, making the tuning of the circuit more complicated, as we must now tune effective parameters and not the explicit ones which appear in Eq. (2). This is, however, not unusual for SQCs, and we can chose a regime where these effects are suppressed and the circuit implements the desired dynamics with a high fidelity as we show below. However, even in this regime, where the dynamics mainly take place in the spin-1/2 subspace, there will still be the important question of the exact effect of the higher levels in the anharmonic oscillator degrees of freedom, both for effective interactions and leakage [54, 73, 81–88]. Below we will

include higher levels in our simulations to judge the impact directly and show the regimes necessary to reduce these effects. We discuss further the effects of the Z-type couplings, tuning, and the working regime for the circuit further in the Methods section.

In order to achieve a staggered mass for the matter site spins, and no mass-like term for the gauge link spin, we use an approach from Ref. [62]. Let  $H_s = H_0 + H_{\text{int}}$ , where  $H_0$  contains all the Z-type terms and  $H_{\text{int}}$  is just the XXX-coupling. Consider  $H_s$  in a frame rotating with respect to  $H_0 + \frac{1}{2}m(\sigma_0 - \sigma_1)$

$$\begin{aligned} H_R &= e^{iH_0 t} (H - H_0) e^{-iH_0 t} \\ &= -\frac{1}{2}m\sigma_0^z + \frac{1}{2}m\sigma_1^z + J_{0g1}^x \sum_{p,r,s \in \{+, -\}} e^{-i\omega_{prs}t} \sigma_0^p \sigma_g^r \sigma_1^s \end{aligned} \quad (3)$$

where the sum is over all eight combinations of the three  $\sigma_i^\pm$ , and the frequency of their phase is given by

$$\omega_{prs} = p(\Omega_0 - m) + r\Omega_g + s(\Omega_1 + m) + 2prsJ_{0g1}^z \quad (4)$$

If the system is now to tuned such that for example  $\omega_{++-} = -\omega_{--+} = 0$ , then the operator  $\sigma_0^+ \sigma_g^+ \sigma_1^- + \text{H.c.}$  will be resonant, as desired. All other combinations will be off-resonant, and would disappear in a RWA, as long as the spin transition frequencies and their differences are much larger than the  $J^z$ , which is already something we must fulfil to justify the truncation to the spin- $\frac{1}{2}$  subspace, see the Methods section. Furthermore, we have recovered the staggered mass via the terms  $-\frac{1}{2}m\sigma_0^z + \frac{1}{2}m\sigma_1^z$ . Thus in an appropriately rotating frame, the Hamiltonian in Eq. (2) implemented by the circuit indeed recreates the one-dimensional U(1) quantum link model of Eq. (1) for two matter sites and the link between them.

In finding appropriate circuit parameters, we optimize according to the effective spin model parameters in order to compensate for the effects of the higher levels. We then do a check of the overall behaviour of the circuit, ensuring that it works as intended, including no significant surviving interactions with higher levels. To do this we use average fidelity [72]. In the Methods section we explain how our use of the average fidelity gives a direct comparison of the time evolution operators of circuit and the target system, described in the previous, while taking into account the higher levels of the circuit.

While we have explained how the XXX-coupling in a RWA yields the desired U(1) interaction term, we do not actually use this approximation, but instead retain all terms to show that they do indeed not disturb the desired dynamics significantly. As mentioned, we present the specific set of optimized circuit parameters which is used in these simulations in the Supplemental Information. All simulations are performed without including noise. However, with present superconducting qubit life times [74, 89, 90] we do not believe noise would significantly disturb the results presented here. In Fig. 2 the calculated average fidelity of the circuit's implementation of the target dynamics can be seen in black. The

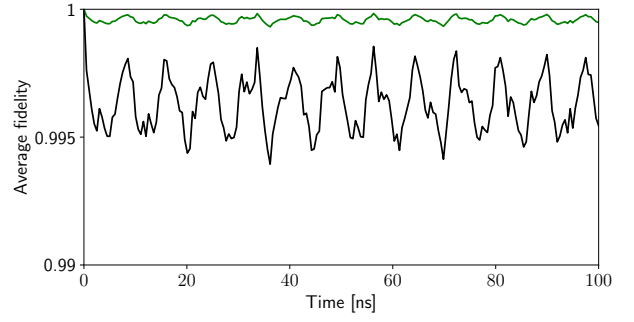


Figure 2. In black: The average fidelity of the circuit's implementation of the target dynamics in a rotating frame. The fidelities are close to or above 99.5% and keep steady over long times, with an oscillation on a short time scale. In green: The fidelity without taking leakage to the higher levels into account. From this we see that the largest part, 0.2–0.45%, of the lost fidelity is due to population immediately leaking into the higher levels and then partly oscillating back and forth. A smaller contribution, about 0.05%, is from the effective interactions induced by virtual processes involving the higher levels.

fidelity is about or above 99.5% at all times, and while it oscillates on a short timescale, it seems to keep steady over the plotted interval. Hence, the implementation of the desired dynamics is good, and stable in the sense that we are not accumulating error or continuously losing population to the higher levels. We seem to lose a small fraction of the population immediately, which then partly oscillates back and forth. In green is plotted the same average fidelity plus the leakage to higher levels, i.e. this plot shows the fidelity if we do *not* take leakage into account. Hence, we can see that about 0.2–0.45% fidelity is lost because of population leaking to the higher levels of the circuit, while about 0.05% is lost due to effective interactions induced by virtual processes involving the higher levels. These high and steady fidelities show directly how our superconducting circuit truly implements the desired dynamics, with circuit parameters available to experiments. Hence, the circuit is a strong candidate for studying the U(1) QLM with present, NISQ-era devices.

The circuit design principles we have used here, i.e. looking at the eigenmodes of the capacitive network in a symmetric circuit to achieve multi-body couplings and suppressing as many undesired interactions as possible, could be used to achieve other interesting gauge invariant systems. It would be an obvious next step to work towards higher gauge symmetries, like SU(2), or to attempt to implement gauge link operators with three levels. The latter would allow for the study of confinement, and might be implemented by using two spin-1/2's to represent one gauge field.

### C. Readout for state tomography

To perform readout of the circuit we would use a method inspired by Refs. [55, 56]. Here they perform quantum state tomography of two qubits by measuring the dispersive shift of a resonator coupled to just one of them. The idea is that strong ZZ-couplings shift the energy of one qubit conditioned on the state of the other sufficiently such that it can be seen in the dispersive shift of the resonator. Hence, where normally one observes two shifts of the resonator corresponding to the two eigenvalues of  $\sigma^z$ , one would see four shifts corresponding to the four combinations of eigenvalues from the two qubits. Similarly, we imagine doing readout of just the matter site spins, but still gain information about the gauge link spins. A resonator coupled through identical capacitors to the two nodes pertaining to a matter site mode (the red and blue branches in Fig. 1) will couple to only that mode. Hence, usual dispersive readout of the spin can be performed. The ZZ-couplings between this mode and its neighbouring gauge and matter modes will make it possible to derive some information about them as well. It is easier to couple to the matter modes, as they live on a single branch between two nodes, while the gauge modes live on four branches between four nodes. We therefore propose measuring on all matter modes and comparing the data to extract information about the whole system.

In the next section we consider quench dynamics of Eq. (1), finding DQPTs using the Loschmidt amplitude  $\mathcal{G}(t) = \langle \psi(0) | \psi(t) \rangle$  (i.e. the overlap between the initial and time-evolved state). An important thing to note is that this quantity in the circuit's own frame will not be the same as in the rotating frame. This is essentially because it involves an odd number of time evolution operators. Transforming to a rotation frame via  $|\psi(t)\rangle \rightarrow U(t)|\psi(t)\rangle$ , for some unitary, time dependent operator  $U(t)$ , the Loschmidt amplitude transforms as  $\langle \psi(0) | \psi(t) \rangle \rightarrow \langle \psi(0) | U(t) | \psi(t) \rangle$ . These two are not identical. However, the Loschmidt amplitude is often measured by performing state tomography [91–95] and then calculating  $\mathcal{G}(t)$  from the results [21, 23–26, 32]. With full information about the state of the circuit at any time, the Loschmidt amplitude can easily be calculated. In our case we have  $U(t) = e^{iH_{0,\text{eff}}t}$ , where  $H_{0,\text{eff}}$  is an effective version of  $H_0$ , taking renormalization from higher level interactions into account.  $H_{0,\text{eff}}$ , which describes the effective energies, could be determined in a separate experiment, by setting  $E_s = 0$  via flux tuning, thus turning off the XXX-coupling, and then initializing in each of the spin-1/2 states, which would then be very close to eigenstates of the system, such that their phase over time would yield their effective energy. An alternative to performing full state tomography is to have multiple copies of the circuit, perform the quench experiment in just one of them while initializing the other in the appropriate initial state. The circuits are then connected using some appropriate scheme to make their states interfere, potentially yielding information about the quantities we

are interested in. Such an approach is used in the context of atoms in an optical lattice in Refs. [96, 97] to measure the Rényi entropy. This has in fact been experimentally probed [98–100].

The effective resonance frequency of a resonator dispersively coupled to a transmon qubit is [73]

$$\omega'_r = \omega_r - \frac{g_r^2}{\Delta + \alpha} - \left( \frac{g_r^2}{\Delta} - \frac{g_r^2}{\Delta + \alpha} \right) \sigma^z \quad (5)$$

Here  $\omega_r$  is the bare resonance frequency,  $\sigma_z$  pertains to the qubit,  $\Delta = \omega_q - \omega_r$  is the detuning between the transition frequency  $\omega_q$  of the qubit and  $\omega_r$ ,  $\alpha$  is the anharmonicity of the qubit, and finally  $g_r$  is the strength of the dispersive coupling. The transition frequency  $\omega_q$  is in our case a combination of the bare spin transition frequency and ZZ-coupling strengths. If we consider coupling a resonator to spin 0 in  $H_s$  of Eq. (2), then we can see that

$$\omega_q = \Omega_0 - 2(J_{0g}^z \sigma_g^z + J_{01}^z \sigma_1^z + J_{0g1}^z \sigma_g^z \sigma_1^z)$$

where the operators are to be understood as the specific eigenvalue they take on in the state that the circuit has collapsed to as we measured it. We can now consider the dispersive shift  $\chi_{ijk} = \omega'_r - \omega_r$  of the resonator frequency as a function of the bare detuning  $\Delta_0 = \Omega_0 - \omega_r$ , where  $i, j, k = 0, 1$  refers to whether spin 0,  $g, 1$  has collapsed to  $|0\rangle$  or  $|1\rangle$ . In Fig. 3 the eight shifts, corresponding to the eight spin-1/2 states of the circuit, for both coupling to spin 0 and 1 are plotted, using the same circuit parameters as above in Fig. 2. We now want to find values of  $\Delta_0$  and  $\Delta_1$  (with  $\Delta_1$  the equivalent of  $\Delta_0$  for the second spin and resonator) such that the eight shifts are as distinct as possible, and where comparing shifts from both of the spins helps to determine the state of the gauge link spin in addition to the two matter site spins. In order to remain in the dispersive region we must satisfy  $g_r/|\Delta|, g_r/|\Delta + \alpha| \ll 1$  where  $\Delta$  now has a different value for each of the spin-1/2 states according to the eight values of  $\omega_q$ . Looking at Eq. (5), we can see that  $\chi_{ijk} \sim g_r^2/|\Delta|, g_r^2/|\Delta + \alpha|$ , and thus the conditions for the dispersive regime can be written as  $\chi_{ijk} \ll g_r$ . This essentially means we must stay well away from the regions where  $\chi_{ijk}$  diverges. These are marked with vertical dashed lines in Fig. 3. If for the sake of example we consider a resonator coupling strength of  $g_r = 20 \times 2\pi\text{MHz}$ , we get the energy scale shown on the right  $y$ -axis of Fig. 3. In the insets of Fig. 3 can be seen zoomed in regions which are between  $\chi_{ijk} = \pm 4 \times 2\pi\text{MHz}$ . If we choose a bare detuning within these regions, we could use the shift of the first resonator (the left inset) to distinguish between the dashed and solid lines, i.e. the state of spin 0, and use the second resonator (the right inset) to distinguish between the blue/navy and the red/brown lines, i.e. the state of spin 1. This is similar to dispersive measurement of qubits, but we can then use this information to exclude some of the theoretical predictions of the measurements, making it easier to distinguish between the shifts caused

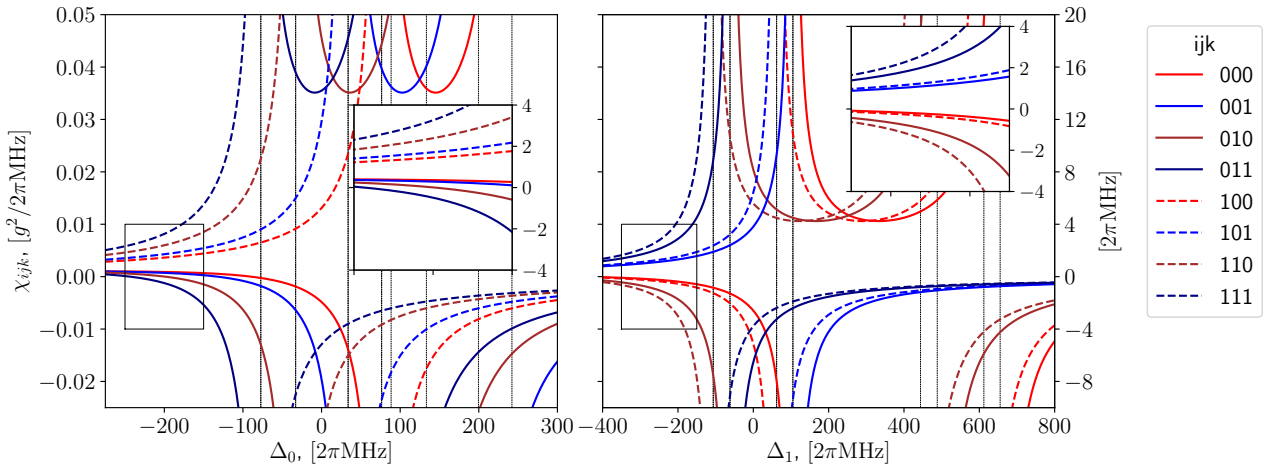


Figure 3. Left and right, the shift  $\chi_{ijk}$  of the resonance frequency of a resonator dispersively coupled to spin 0 or spin 1, respectively, for all eight spin-1/2 states of the circuit. The shifts are plotted as functions of the bare detuning  $\Delta_n = \Omega_n - \omega_r$  for  $n = 0, 1$  respectively. The indices  $ijk = 0, 1$  denote the state,  $|0\rangle$  or  $|1\rangle$ , of each of the three spins. Assuming a resonator coupling strength of  $g_r = 20 \times 2\pi\text{MHz}$ , we get the energy scale shown on the right  $y$ -axis. The insets show intervals of the bare detunings where the dispersive shifts of each state are distinct enough to distinguish between the eight spin state with just these two measurements, particularly when the information from each measurement is compared. To be in the dispersive regime we must have  $\chi_{ijk} \ll g_r$ , i.e. we must stay well away from the points where  $\chi_{ijk}$  diverges, which are marked with vertical dashed lines.

by the state of the gauge link spin. With a resolution of  $1 \times 2\pi\text{MHz}$  in a measurement of the dispersive shift, which is experimentally feasible [24, 55, 56, 101], it would be possible to distinguish the states of the circuit with this or even a smaller choice of  $g_r$ .

The above analysis is approximate, as it uses only the bare spin model parameters, and the formula Eq. (5) is derived for a single qubit with some specific bare transition frequency coupled to a resonator. In our case it is clear that the higher levels of the circuit would affect these calculations, and it is in fact a resonator, or several, coupled to a larger circuit, a system of multiple interacting qubits or spins. A more accurate analysis using numerical methods could be carried out to find the actual shifts of the resonance frequency of the resonator dependent on the circuit state. However, the quantitative results would be the same, namely that the different states would result in different shifts. It would then be a matter of determining whether those shifts would be sufficient to distinguish the states in a measurement, using the comparative method outlined above. Whether or not this is the case is in the end a consequence of the chosen circuit parameters, so one could optimize the circuit parameters with respect to these considerations. These dispersive readouts could then be used to perform a full quantum state tomography, yielding all information necessary to study the dynamics of the system.

#### D. DQPTs in QLM chain

A recent study by Zache et al. has considered DQPTs in continuum and LGT models. In Ref. [30], DQPTs were found through the study of vorticity in an appropriate order parameter, implying that the transitions have a topological nature. Here, we consider the QLM equivalent of their system, described by Eq. (1), over a larger range of parameters and write down a gauge invariant string order parameter as an example of what the above proposed realization of a spin-1/2 QLM could be used to study. We show how the zeros of both this order parameter as well as those of the Loschmidt amplitude  $\mathcal{G}(t)$ , following a quench of the sign of the mass term,  $m \rightarrow -m$ , can be found by looking for vortices in their respective phases in the Methods section. Hence, there is a topological aspect to the DQPTs we observe, both through the order parameter, but also directly in the Loschmidt amplitude. The vortices of the order parameter are dynamical in the sense that as a function of the matter-gauge interaction strength, they are created, move around, and can annihilate with each other [32]. We find that the Loschmidt echo  $\mathcal{L}(t) = |\mathcal{G}(t)|^2$  and its zeros, corresponding to the zeros of the Loschmidt amplitude  $\mathcal{G}(t)$  itself, converge to a certain structure for larger system sizes, particularly for small times. The zeros appear to be converging to lines in the thermodynamic limit. Similar results have been found in other systems with DQPTs, and is similar to how the zeros of a partition function are known to converge to lines in the thermodynamic limit [10, 15, 28, 102].



This quench corresponds to a maximal quench of the vacuum angle. The vacuum angle is a parameter that may be included in Quantum Chromodynamics as well as the Schwinger model, relating to the non-trivial structure of their vacua [103, 104], and quantifying a CP-violating term. For more information see [59, 103–110]. We will, however, not be considering the vacuum angle itself, but will rather focus on the quench, and the subsequent DQPTs. Explicitly we will be initializing the system in the ground state of the pre-quench Hamiltonian  $H_i = H(m, J)$  at time  $t = 0$ , and then perform unitary time evolution according to the post-quench Hamiltonian  $H_f = H(-m, J)$ . We then study the Loschmidt amplitude, and Loschmidt echo  $\mathcal{L}(t) = |\mathcal{G}(t)|^2$  (the zeros of these quantities *define* the occurrence DQPTs), as well as a both spatially and temporally non-local order parameter  $g(k, t) = \langle \psi(0) | \mathbf{g}(k) | \psi(t) \rangle$  that we introduce, where  $\mathbf{g}(k)$  is the Fourier transform of the gauge invariant string order parameters of the system, which we discuss further in the Methods section. We study the dynamics of the Loschmidt amplitude and the order parameter for different system sizes,  $N = 2, 4, \dots, 18$ .

This novel order parameter has zeros along the troughs of the Loschmidt echo,  $\mathcal{L}(t)$ , for all system sizes. As mentioned these zeros are accompanied by vortices in the phase of the order parameter, which can be counted by a winding number (see the Methods section). Hence, even in the smallest system this order parameter reveals the structure of  $\mathcal{L}(t)$ , which repeats itself as the system size is increased, and exhibits non-trivial vortex dynamics. The order parameter that we employ here is related to the gauge-invariant time-ordered Green's function computed in the context of lattice gauge theory in [30] and our work demonstrates how to transfer this to QLM models.

In Fig. 4 can be seen  $\mathcal{L}(t)$  for the considered range of  $J/m$  and  $t$ , for system sizes  $N = 4, 8, 16$ . The zeros of  $\mathcal{L}(t)$  are marked with circles colour-coded according to the orientation of the vortices, i.e. whether they wind upwards counter-clockwise or clockwise, corresponding to being right- or left-handed. It is unclear whether the orientation of the vortices in the phase of  $\mathcal{G}(t)$  has any significance. Most of them are left-winding with a few right-winding at late times in the middle and lower frames of Fig. 4. The zeros of  $\mathcal{L}(t)$  are found by applying the method described above to the phase,  $\phi_{\mathcal{G}(t)}$ , of  $\mathcal{G}(t)$ . This phase has two components  $\phi_{\mathcal{G}(t)} = \phi_{\text{dyn}} + \phi_P$ , where  $\phi_{\text{dyn}}$  is the dynamical phase defined by  $\phi_{\text{dyn}} = -\int_0^t dt' \langle \psi(t') | H_f | \psi(t') \rangle = -t \langle \psi(0) | H_f | \psi(0) \rangle$ , while the  $\phi_P$  is a purely geometric phase called the Pancharatnam geometric phase [111], which is an extension of the concept of Berry's phase [21, 111, 112]. It is the Pancharatnam phase which contains the vortices, while the dynamical varies smoothly as a function of  $J/m$  and is linear in  $t$ .

The zeros of the order parameter are indicated with triangles and a different colour code for distinguishability. We can see how the zeros of the order parameter lie along the troughs of  $\mathcal{L}(t)$ . Intuitively, one might think of

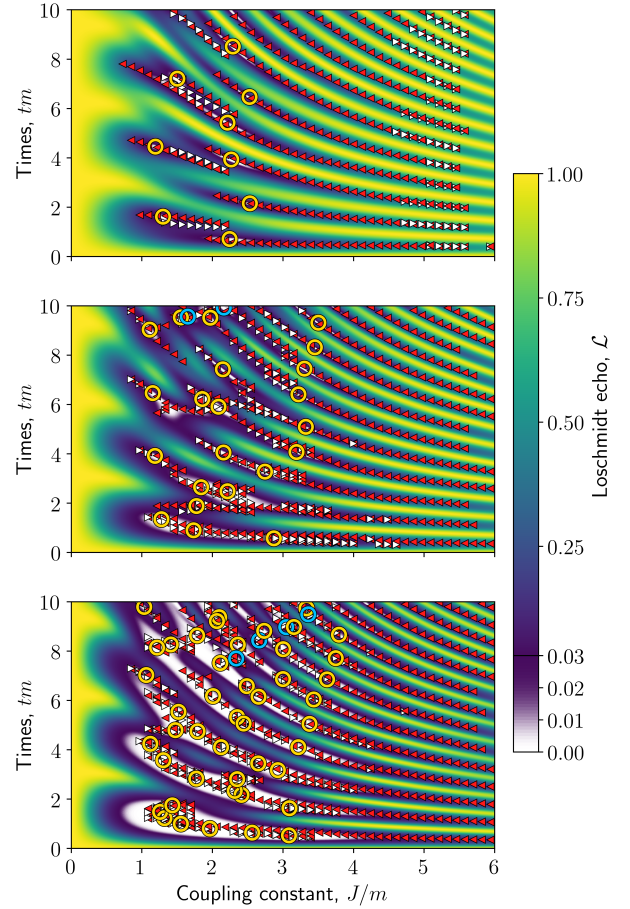


Figure 4. Contour plots of  $\mathcal{L}(t)$  for the considered range of  $J/m$  and  $t$ , for system sizes  $N = 4, 8, 16$  from top to bottom. The zeros, as found by considering vortices in the phase of  $\mathcal{G}(t)$ , are marked with circles coloured blue for right-winding vortices, and yellow for left-winding. A representative set of the vortices of the order parameter are plotted with arrow heads. White arrow heads pointing to the right indicate right-winding vortices, and red arrow heads pointing left indicate left-winding vortices. These trace out the continuous lines in the  $(J, t)$ -plane where the order parameter vanishes. Particularly for  $N = 4$  in the top panel it can be clearly seen how vortices of opposite orientation move around the  $(J, t)$ -plane and annihilate. The structure of  $\mathcal{L}(t)$  and its zeros has a clear pattern that is present in all three plots. For  $N = 16$   $\mathcal{L}(t)$  is very close to zero in large areas, and its zeros, particularly at early times, trace out a curve following the center of these lobes.

the vortices as charges, and when two charges of opposite sign are near each other, they screen each other off, allowing them to be in areas where  $\mathcal{L}(t)$  takes on larger values. For  $N = 4$  in the upper panel of Fig. 4 it is particularly clear in for example the region  $1 < J/m < 2$ , how vortices in the phase of the order parameter of opposite orientation are created as a pair, move in the  $J, t$ -plane, and annihilate with each other. Furthermore, we see how

the order parameter does not have zeros for very small and very large  $J/m$ . Intuitively it is reasonable that for both  $J/m \ll 1$  and  $J/m \gg 1$  we would not see any zeros in the order parameter, as a weak coupling would make the dynamics too slow for zeros to appear in the time we simulate, and a very strong coupling would make the mass, and as such the quench of it, become insignificant. A similar conclusion was reached in [30].

There is a clear pattern of  $\mathcal{L}(t)$  being small in large lobes that start at around  $J/m = 0.5$  and stretch towards higher  $J/m$  while  $\mathcal{L}(t)$  increases. The zeros of  $\mathcal{L}(t)$  occur near the center of these lobes. This pattern appears already at  $N = 4$  and repeats itself for larger system sizes. We thus see how even the small system with  $N = 4$  reproduces features of the much larger  $N = 16$  system, where the behaviour of  $\mathcal{L}(t)$  has started to converge. This means that even a small experimental realization of this system could yield interesting results. While the even smaller system with  $N = 2$  does show zeros both in  $g$  and  $\mathcal{L}(t)$  the behaviour of these is considerably different and simpler than for larger  $N$ . We explain this different behaviour by its small size. Its dynamics are necessarily quite different simply because it is so limited. Hence, while that system may be interesting for experimental studies in itself, it does not reflect the behaviour of large  $N$  systems as well as  $N = 4$  does. In a future work we will elaborate on our results regarding this quench of a U(1) QLM.

From the above we see how this system hosts non-trivial post-quench dynamics, and how even a small version of the system reflects the behaviour of a much larger version. This makes it relevant for experimental study using the SQC we proposed above. Using quantum state tomography with the proposed method of measurement, all information necessary for calculating the Loschmidt amplitude and our order parameter could be extracted to study the small version of the system.

### III. DISCUSSION

We have shown how to realize lattice gauge theories in superconducting quantum circuits. Specifically, we have provided a method for general circuits to implement quantum link models with a high average fidelity. This opens up the possibility for experimental study of quantum link models in NISQ-era devices. We have proposed a superconducting circuit, which realizes three spin-1/2's interacting via a direct XXX-coupling, which through appropriate tuning becomes the matter-gauge interaction necessary for a U(1) quantum link model. The circuit can be modularly scaled in an intuitive way and realizes the desired U(1) QLM dynamics with an average fidelity of about 99.5% or above, using realistic circuit parameters. We have proposed an approach for read-out of the circuit, using a method of resonators coupled dispersively to a subset of the circuit spins, but which nonetheless gives information about all the spins, by ex-

plotting their pairwise ZZ-couplings. Using the same set of circuit parameters again we showed how this method can principally reduce the complexity of measurement of the circuit's state.

As a demonstration of the principles in our work we have studied a periodic (1+1)D spin-1/2 quantum link model with local U(1) gauge symmetry, corresponding to the Schwinger model. Even with the smallest lattice considered the system undergoes dynamical quantum phase transitions after a quench of the sign of the mass. We studied an order parameter, which is essentially the Fourier transform of the gauge invariant string order parameter, which had zeros that correlated with the minima of the Loschmidt amplitude and its zeros. The zeros of both the Loschmidt amplitude and our complex order parameter were found by looking for vortices in their phases, which are much easier to find numerically, as they are extended structures. We will elaborate on our results regarding this system in future work.

As an extension of this work it would be interesting to study dynamics of more complicated lattice configurations and gauge theories. For example periodic 2D, i.e. toric, QLMs could be considered, which would likely show interesting topological aspects. Additional degrees of freedom could be added to the link operators, indeed simply promoting them to spin-1's would allow for the study of confinement and pair production. It would be natural to work towards a superconducting circuit realization of such models using the same design principles we have presented here. A similarly modular circuit realizing SU(2) symmetric interactions between fermions, or some other interesting gauge symmetry like  $\mathbb{Z}_n$  would be interesting to develop. Further work could also be done on the specific system studied here. It would be interesting to link the dynamical quantum phase transitions found here to a potential underlying equilibrium phase transition or entropy production [19, 21, 23].

### IV. METHODS

#### A. Circuit Hamiltonian

We will here give a few details on the derivation of the spin Hamiltonian of our circuit, as shown in Fig. 1. We define the node fluxes of the circuit  $\phi = (\phi_1, \phi_2, \phi_3, \phi_4)^T$  [57], but will be working in the eigenmodes of the capacitive network [53–56, 81],  $\psi = (\psi_{CM}, \psi_0, \psi_g, \psi_1)^T$ , defined through

$$\phi = \begin{pmatrix} 1 & 1 & \frac{1}{2} & 0 \\ 1 & -1 & \frac{1}{2} & 0 \\ 1 & 0 & -\frac{1}{2} & 1 \\ 1 & 0 & -\frac{1}{2} & -1 \end{pmatrix} \psi$$

This results in no interactions through the capacitors, greatly reducing the complexity of the interactions in the system. We will furthermore introduce a new set of external fluxes,  $\Psi_0, \Psi_g$  and  $\Psi_1$ , of which the  $\Phi_i$  are certain



simple, linear combinations. We set these new external fluxes to be constant  $\Psi_j = -\pi/2$  for  $j = 0, g, 1$ . In these coordinates and with these choices of external fluxes the circuit Hamiltonian becomes

$$\begin{aligned}
H_c = & \frac{\mathcal{K}_{00}^{-1}}{2} q_0^2 + \frac{\mathcal{K}_{gg}^{-1}}{2} q_g^2 + \frac{\mathcal{K}_{11}^{-1}}{2} q_1^2 \\
& - E_0 \cos \psi_0 - E_1 \cos \psi_1 \\
& - 4E_c \cos \psi_0 \cos \psi_g \cos \psi_1 \\
& - 4E_s \sin \psi_0 \sin \psi_g \sin \psi_1
\end{aligned} \tag{6}$$

where the  $q_j$  are momentum variables conjugate to the  $\psi_j$ , and  $\mathcal{K}_{jj}^{-1}$  are the diagonal entries of the inverse capacitance matrix in the  $\psi_j$  coordinates. This Hamiltonian describes three transmon-like [73] anharmonic oscillator modes, interacting only through the interesting triple cosine and sine interactions. These are direct, completely even and completely odd, three-body interactions. The sine functions come about as a consequence of setting  $\Psi_j = -\pi/2$ . Recasting each of the  $\psi_j$  and  $q_j$  variables in terms of harmonic oscillator operators, i.e. bosonic creation and annihilation operators,  $a_j^\dagger$  and  $a_j$ , and truncating the system to the two lowest levels of each, yields the spin Hamiltonian in Eq. (2). This shows how the  $\psi_0$ - and  $\psi_1$ -modes will represent matter site spins, while the  $\psi_g$ -mode has the role of gauge link spin. For a full derivation of the Hamiltonian, and explicit expressions for the spin model parameters, see the Supplemental Information.

## B. Z-type couplings and working regime

Though the Z-type couplings in Eq. (2) are principally undesirable, their effect is mainly to make the tuning of the circuit slightly more complicated. They do not disturb the main and interesting feature of the system. Looking at the Hamiltonian, the Z-type couplings essentially just shift the energy levels of the system, but it turns out that this does not affect the detuning of the states we are interested in, except for the ZZZ-coupling which, however, is a weak coupling. More importantly, however, is the fact that the coupling strengths of the Z-type couplings are representative for even interactions between the spin-1/2 subspace and higher levels of the circuit. These are interactions like  $a_j^\dagger a_j^\dagger a_{j'} a_{j'} + \text{H.c.}$  or  $a_j^\dagger a_j^\dagger a_{j'}^\dagger a_{j'}^\dagger + \text{H.c.}$ , where there is an even number of creation and annihilation operators,  $a_j^\dagger$  and  $a_j$ , for each anharmonic mode. When working in the spin-1/2 subspace, where each mode has at most *one* excitation, these interaction will either simply have no effect because they can not remove two excitations from the modes, or they will be suppressed if the coupling strengths are much smaller than the spin transition energies. However, higher order contributions from such interactions will turn out to affect both the detuning of  $|1_0 1_g 0_1\rangle$  and  $|0_0 0_g 1_1\rangle$ , and the strength of the XXX-coupling. That is, the system will

undergo virtual excitations and de-excitations, which effectively change the spin model parameters. Again, this does not disturb the main feature of the circuit, but simply renormalizes the parameters, making the tuning of the circuit more complicated, as we must now tune effective parameters and not the bare ones which appear in Eq. (2). Specifically, we are interested in tuning  $|1_0 1_g 0_1\rangle$  and  $|0_0 0_g 1_1\rangle$  into resonance, with all other states detuned. Because of the staggered mass in Eq. (1), the first of these two states represents a particle-antiparticle pair connected by a gauge field flux tube, and the second represents two empty sites with the gauge field pointing the opposite direction. If these are in resonance while all others are not, the XXX-coupling will implement the proper gauge invariant interaction, reducing to  $\sigma_0^+ \sigma_g^+ \sigma_1^- + \text{H.c.}$ . This corresponds to  $\omega_{++-} = -\omega_{--+} = 0$ , as discussed below Eq. (4).

Though the Z-type couplings would all disappear by setting  $E_c = 0$ , i.e. removing the junctions pertaining to  $E_c$ , this would result in the anharmonicity of the gauge link mode vanishing. The anharmonicities  $\alpha_j$  of the three modes, which justify the truncation to the two lowest level of each anharmonic oscillator, can be seen in the Supplemental Information. We note that  $\alpha_g$  is indeed proportional to  $E_c$ , because the gauge link mode is only affected by the Josephson junctions on the purple branches. The anharmonicities of the matter site modes,  $\alpha_0$  and  $\alpha_1$ , each have contributions from both  $E_c$ , and  $E_0$  or  $E_1$  respectively. The truncation is justified if interactions between the spin- $\frac{1}{2}$  subspace and higher levels of the Hilbert space of Eq. (2) are suppressed. This will, briefly put, be the case if even interaction strengths are much smaller than spin transition frequencies and their differences, and if odd interaction strengths are much smaller than the anharmonicities, i.e. for our system if  $J^z \ll \Omega_j$  and  $J_{0g1}^x \ll \alpha_j$ .

## C. Comparison of circuit and target dynamics

To compare the dynamics of our circuit, as described by Eq. (6), with the target dynamics, described by Eq. (1), we use average fidelity. Average fidelity is a measure of how well a certain process implements a desired operation. In our case the process is the time evolution of the circuit, determined by the full circuit Hamiltonian in Eq. (6), in a frame rotating such that the resulting Hamiltonian is  $H_R$  in Eq. (3), where  $m$  is set to half the effective detuning between  $|1_0 1_g 0_1\rangle$  and  $|0_0 0_g 1_1\rangle$  (here 0 and 1 refer to the ground and excited state of the spin, and the subscripts denote which spin it is), and the bare coupling strength  $J_{0g1}^x$  is replaced with the effective coupling between these two states. To take contributions beyond renormalized parameters from higher level interactions into account, we truncate the anharmonic modes of the circuit to the lowest *four* levels, when simulating dynamics. We only rotate the spin-1/2 states, i.e. we use a four-level version of  $H_0 + \frac{1}{2}m(\sigma_0 - \sigma_1)$ , where all en-

tries pertaining to levels higher than the spin-1/2 states are just zero. The operation we compare this with is the time evolution according to the target Hamiltonian, i.e.  $H$  from Eq. (1) with two matter sites and a gauge link between them. We compare only the dynamics of the spin-1/2 states, i.e. time-evolution of the circuit takes place with four levels included for each mode, with the spin-1/2 states rotated, and the result is then projected down to the spin-1/2 subspace, before comparing with the time-evolution of  $H$ . For details on how the average fidelity is calculated, using the clever formula of Ref. [72], see the Supplemental Information. The average fidelity thus compares the very time evolution operators themselves for the circuit and the target system. Following our analysis, and as the mass and coupling strength of the target Hamiltonian are chosen to be half the effective detuning and the effective coupling strength respectively, the fidelity is *a priori* expected to be quite high. Since this is all done with four levels included in each anharmonic mode, the fidelity will, however, be a measure of how much the higher levels affect the dynamics of the circuit beyond just the renormalization of the mass and coupling strength. In particular, some population will be lost to the higher levels, and just as virtual processes contribute to the strength of the XXX-coupling, they will also to some extent induce other effective interactions. These will disturb the desired dynamics and might be gauge variant, resulting in population moving outside of the chosen gauge sector of the spin-1/2 subspace. As can be seen in Fig. 2 the circuit implements the desired dynamics with a very high and steady fidelity.

### D. Order parameter

Our order parameter is  $g(k, t) = \langle \psi(0) | \mathbf{g}(k) | \psi(t) \rangle$ , where  $|\psi(t)\rangle$  is the state at time  $t$  and

$$\mathbf{g}(k) = \sum_{m=0,1} \sum_{n=0}^{N-1} e^{-ikd_m(n)} \sigma_m^- \prod_{i=m}^{n-1} S_{i,i+1}^{\alpha_m(n)} \sigma_n^+$$

This is a sum over two representative sites  $m = 0, 1$  (a particle site and an antiparticle site), and over all sites of the lattice  $n = 0, \dots, N-1$ . The summand is a Fourier coefficient times a string operator, consisting of two matter site operators, one at the representative site  $m$  and the other at  $n$ , connected by the gauge link operators between the two sites, making the total operator gauge invariant. Here the products of link operators are over the *shortest* path between site  $m$  and site  $n$ , i.e. either counter-clockwise or clockwise along the circular lattice, see Fig. 5. Likewise  $d_m(n)$  is the distance from site  $m$  to  $n$  along the shortest path, with  $d_m(n)$  being positive for clockwise paths and negative for counter-clockwise paths. Similarly,  $\alpha_m(n) = -$  for clockwise paths and  $\alpha_m(n) = +$  for counter-clockwise paths, ensuring the gauge invariance of the summands. For sites on the exact opposite side of the circular lattice, i.e.  $m - n = N/2$ , the two

paths around the lattice are equidistant and so *both* are included, see Fig. 5b. Thus the operator  $\mathbf{g}(k)$  is essentially the Fourier transform of the gauge invariant string operators connecting the sites 0 and 1 with all sites of the lattice. The order parameter  $g(k, t)$  is then the Fourier transform of the amplitudes of a matter excitation moving from either site 0 or 1 to site  $n$ , via the shortest path, in the time between initialization and  $t$ , in a gauge invariant manner. The reason we have both a term for site 0 and one for site 1 is to make the operator symmetric with respect to particles and antiparticles, as site 0 is a particle site while site 1 is an antiparticle site.

### E. Counting vortices

Considering  $\mathcal{G}(t)$  as a complex function in the  $(J, t)$ -plane and  $g(k, t)$  a complex function in the  $(k, t)$ -plane (with  $J$  fixed), we can find their zeros in a similar fashion, namely by looking at their phase. Zeros of a smooth complex function of two variables are accompanied by vortices in the phase of that function. This leads to a method for numerically finding the vortices as detailed below, which is an adaptation of the work in Ref. [113], developed for computing Chern numbers in momentum space. When a complex function, say  $f = re^{i\varphi}$ , becomes zero at some critical point, its phase  $\varphi$  is undefined at that point. For a smooth function of two variables,  $f = f(x, y)$ , this results in a vortex in  $\varphi$  surrounding the critical point. The intuition of this is that while  $\varphi$  is undefined at the critical point it is otherwise smooth, up to discontinuities of  $2\pi$ . If there were no discontinuity around the critical point there would obviously be a meaningful, smooth extension of  $\varphi$  at the undefined point, which contradicts the fact that  $f$  goes to zero. The phase must thus have a line of  $2\pi$  discontinuity extending from the critical point, which we will refer to as tears (as in torn fabric). Starting at this discontinuity and going around the critical point,  $\varphi$  must then attain all possible values between  $-\pi$  and  $\pi$  in a smooth way, as there would otherwise again be a meaningful, smooth extension of  $\varphi$ , or discontinuities with a different value than  $2\pi$ . Hence, going around the critical point in a closed curve,  $\varphi$  will go through all values from  $-\pi$  to  $\pi$ , and have a discontinuity of  $2\pi$  between the extremal values. Such vortices can be counted by a winding number

$$\nu = \frac{1}{2\pi} \oint_{\mathcal{C}} d\mathbf{l} \cdot \nabla \varphi$$

where  $\mathcal{C}$  is a closed curve. This number may then be considered a dynamical topological order parameter [26, 31], as it is a parameter changing its value with time, taking on discrete values which only depend on the topology of  $\varphi$ , i.e. its vortices, and whether  $\mathcal{C}$  encloses these vortices. Such a winding number essentially detects and counts the number of times  $\varphi$  has discontinuously jumped from  $\pi$  to  $-\pi$  along  $\mathcal{C}$ , minus the number of times  $\varphi$  has jumped from  $-\pi$  to  $\pi$ , i.e. how many times in total  $\varphi$  increases

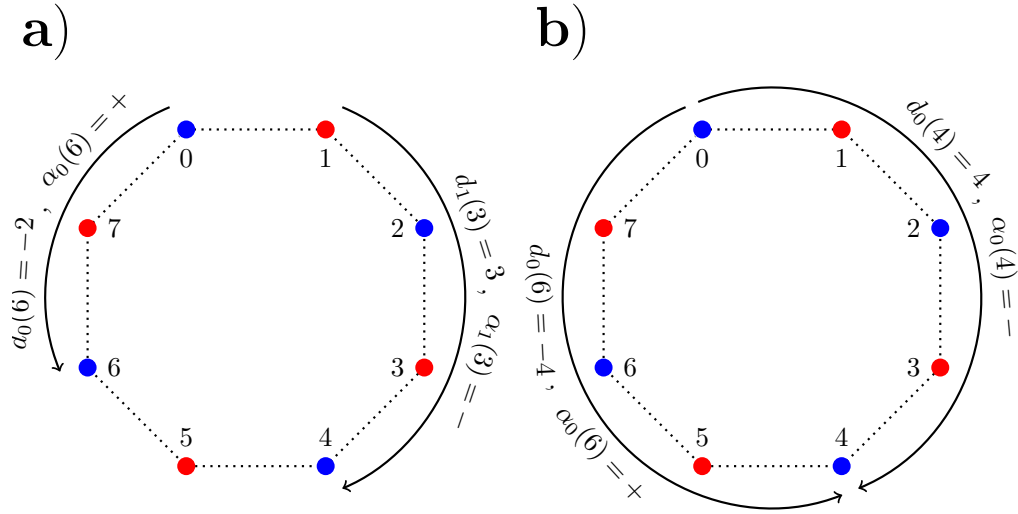


Figure 5. Some examples of the paths taken by the string operators which are summed over in the order parameter for a system size of  $N = 8$  matter sites. a) Two examples, one originating from particle site 0 and the other from the antiparticle site 1, showing the sign conventions for clockwise and counter-clockwise paths. b) An example of the case where  $m - n = N/2$ , where the equidistant clockwise and counter-clockwise paths are both taken into account.

by  $2\pi$  along the closed curve. Hence, closing such a curve tightly around a vortex, the winding number essentially just detects that a tear enters the area enclosed by the curve without exiting again. Together with the image of the vortices always being tailed by these tears, we see that to find the vortices we must simply be able to identify the tears and their ends. The tears can only end either at the edge of the considered parameter space or at a vortex. Hence, one only needs sufficient resolution (in a simulation or data) to distinguish discontinuous jumps of  $2\pi$  from the jumps between the data points on a coarse grid in order to find the zeros of the function  $f$ . This makes it possible to find and study zeros and vortices with a minimal numerical computational effort, and we have used an algorithm based on this idea to do so in our system. Furthermore, one can be certain that these will be true zeros of the function, and not points where the complex function merely has a very small modulus. This is otherwise principally quite hard to do, as unavoidable numerical imprecision would usually make it necessary to set an arbitrary limit on when the modulus is small

enough to indicate that the function has actually become zero. Essentially, the vortices are easy to find numerically even with low resolution because they are extended structures (as opposed to the single point where the function vanishes). This extended nature is also the reason they can be counted by a winding number.

## V. DATA AVAILABILITY

The data that support the findings in this study are available from the corresponding author upon reasonable request.

## VI. CODE AVAILABILITY

All code used to generate the presented data in this paper is available upon reasonable request.

- 
- [1] I. M. Georgescu, S. Ashhab, and F. Nori, Quantum simulation, *Reviews of Modern Physics* **86**, 153 (2014).
  - [2] J. Zhang, P. W. Hess, A. Kyprianidis, P. Becker, A. Lee, J. Smith, G. Pagano, I.-D. Potirniche, A. C. Potter, A. Vishwanath, N. Y. Yao, and C. Monroe, Observation of a discrete time crystal, *Nature* **543**, 217 (2017).
  - [3] S. Choi, J. Choi, R. Landig, G. Kucsko, H. Zhou, J. Isoya, F. Jelezko, S. Onoda, H. Sumiya, V. Khemani, C. von Keyserlingk, N. Y. Yao, E. Demler, and M. D.

- Lukin, Observation of discrete time-crystalline order in a disordered dipolar many-body system, *Nature* **543**, 221 (2017).
- [4] M. Schreiber, S. S. Hodgman, P. Bordia, H. P. Luschen, M. H. Fischer, R. Vosk, E. Altman, U. Schneider, and I. Bloch, Observation of many-body localization of interacting fermions in a quasirandom optical lattice, *Science* **349**, 842 (2015).

- [5] J. Smith, A. Lee, P. Richerme, B. Neyenhuys, P. W. Hess, P. Hauke, M. Heyl, D. A. Huse, and C. Monroe, Many-body localization in a quantum simulator with programmable random disorder, *Nature Physics* **12**, 907 (2016).
- [6] M. Gring, M. Kuhnert, T. Langen, T. Kitagawa, B. Rauer, M. Schreitl, I. Mazets, D. A. Smith, E. Demler, and J. Schmiedmayer, Relaxation and Prethermalization in an Isolated Quantum System, *Science* **337**, 1318 (2012).
- [7] B. Neyenhuys, J. Zhang, P. W. Hess, J. Smith, A. C. Lee, P. Richerme, Z.-X. Gong, A. V. Gorshkov, and C. Monroe, Observation of prethermalization in long-range interacting spin chains, *Science Advances* **3**, e1700672 (2017).
- [8] C. Neill, P. Roushan, M. Fang, Y. Chen, M. Kolodrubetz, Z. Chen, A. Megrant, R. Barends, B. Campbell, B. Chiaro, A. Dunsworth, E. Jeffrey, J. Kelly, J. Mutus, P. J. J. O'Malley, C. Quintana, D. Sank, A. Vainsencher, J. Wenner, T. C. White, A. Polkovnikov, and J. M. Martinis, Ergodic dynamics and thermalization in an isolated quantum system, *Nature Physics* **12**, 1037 (2016).
- [9] E. A. Martinez, C. A. Muschik, P. Schindler, D. Nigg, A. Erhard, M. Heyl, P. Hauke, M. Dalmonte, T. Monz, P. Zoller, and R. Blatt, Real-time dynamics of lattice gauge theories with a few-qubit quantum computer, *Nature* **534**, 516 (2016), [arXiv:arXiv:1605.04570v1](#).
- [10] M. Heyl, A. Polkovnikov, and S. Kehrein, Dynamical quantum phase transitions in the transverse-field ising model, *Physical Review Letters* **110**, 1 (2013), [arXiv:arXiv:1206.2505v2](#).
- [11] M. Heyl, Scaling and Universality at Dynamical Quantum Phase Transitions, *Physical Review Letters* **115**, 1 (2015), [arXiv:arXiv:1505.02352v2](#).
- [12] E. Canovi, P. Werner, and M. Eckstein, First-Order Dynamical Phase Transitions, *Physical Review Letters* **113**, 265702 (2014), [arXiv:1408.1795](#).
- [13] D. Pekker, G. Refael, E. Altman, E. Demler, and V. Oganesyan, Hilbert-Glass Transition: New Universality of Temperature-Tuned Many-Body Dynamical Quantum Criticality, *Physical Review X* **4**, 011052 (2014).
- [14] R. Vosk and E. Altman, Dynamical Quantum Phase Transitions in Random Spin Chains, *Physical Review Letters* **112**, 217204 (2014).
- [15] M. Schmitt and S. Kehrein, Dynamical quantum phase transitions in the Kitaev honeycomb model, *Physical Review B* **92**, 075114 (2015).
- [16] A. A. Zvyagin, Nonequilibrium dynamics of a system with two kinds of fermions after a pulse, *Physical Review B* **95**, 075122 (2017).
- [17] Y.-P. Huang, D. Banerjee, and M. Heyl, Dynamical Quantum Phase Transitions in U(1) Quantum Link Models, *Physical Review Letters* **122**, 250401 (2019), [arXiv:1808.07874](#).
- [18] M. Lacki and M. Heyl, Dynamical quantum phase transitions in collapse and revival oscillations of a quenched superfluid, *Physical Review B* **99**, 1 (2019), [arXiv:1812.02209](#).
- [19] B. O. Goes, G. T. Landi, E. Solano, M. Sanz, and L. C. Céleri, Wehrl entropy production rate across a dynamical quantum phase transition (2020), [arXiv:2004.01126](#).
- [20] A. A. Zvyagin, Dynamical quantum phase transitions (Review Article), *Low Temperature Physics* **42**, 971 (2016), [arXiv:1701.08851](#).
- [21] M. Heyl, Dynamical quantum phase transitions: A review, *Reports on Progress in Physics* **81**, 10.1088/1361-6633/aaaf9a (2018), [arXiv:1709.07461](#).
- [22] M. Heyl, Dynamical quantum phase transitions: A brief survey, *Epl* **125**, 25 (2019), [arXiv:arXiv:1811.02575v1](#).
- [23] P. Jurcevic, H. Shen, P. Hauke, C. Maier, T. Brydges, C. Hempel, B. P. Lanyon, M. Heyl, R. Blatt, and C. F. Roos, Direct Observation of Dynamical Quantum Phase Transitions in an Interacting Many-Body System, *Physical Review Letters* **119**, 080501 (2017), [arXiv:1612.06902](#).
- [24] X. Y. Guo, C. Yang, Y. Zeng, Y. Peng, H. K. Li, H. Deng, Y. R. Jin, S. Chen, D. Zheng, and H. Fan, Observation of a Dynamical Quantum Phase Transition by a Superconducting Qubit Simulation, *Physical Review Applied* **11**, 1 (2019), [arXiv:1806.09269](#).
- [25] K. Xu, Z.-H. Sun, W. Liu, Y.-R. Zhang, H. Li, H. Dong, W. Ren, P. Zhang, F. Nori, D. Zheng, H. Fan, and H. Wang, Probing the dynamical phase transition with a superconducting quantum simulator (2019), [arXiv:1912.05150](#).
- [26] X.-Y. Xu, Q.-Q. Wang, M. Heyl, J. C. Budich, W.-W. Pan, Z. Chen, M. Jan, K. Sun, J.-S. Xu, Y.-J. Han, C.-F. Li, and G.-C. Guo, Measuring a dynamical topological order parameter in quantum walks, *Light: Science & Applications* **9**, 7 (2020), [arXiv:1808.03930](#).
- [27] H. Hu and E. Zhao, Dynamical topology of quantum quenches in two dimensions (2019), [arXiv:1911.02211](#).
- [28] S. Vajna and B. Dóra, Topological classification of dynamical phase transitions, *Physical Review B - Condensed Matter and Materials Physics* **91**, 10.1103/PhysRevB.91.155127 (2015), [arXiv:arXiv:1409.7019v1](#).
- [29] I. Hagymási, C. Hubig, Legeza, and U. Schollwöck, Dynamical Topological Quantum Phase Transitions in Nonintegrable Models, *Physical Review Letters* **122**, 1 (2019), [arXiv:1904.00867](#).
- [30] T. V. Zache, N. Mueller, J. T. Schneider, F. Jendrzejewski, J. Berges, and P. Hauke, Dynamical Topological Transitions in the Massive Schwinger Model with a  $\theta$  Term, *Physical Review Letters* **122**, 1 (2019), [arXiv:arXiv:1808.07885v1](#).
- [31] J. C. Budich and M. Heyl, Dynamical topological order parameters far from equilibrium, *Physical Review B* **93**, 10.1103/PhysRevB.93.085416 (2016), [arXiv:arXiv:1504.05599v3](#).
- [32] N. Fläschner, D. Vogel, M. Tarnowski, B. S. Rem, D.-S. Lühmann, M. Heyl, J. C. Budich, L. Mathey, K. Senostock, and C. Weitenberg, Observation of dynamical vortices after quenches in a system with topology, *Nature Physics* **14**, 265 (2018).
- [33] Z. Huang and A. V. Balatsky, Dynamical Quantum Phase Transitions: Role of Topological Nodes in Wave Function Overlaps, *Physical Review Letters* **117**, 086802 (2016).
- [34] M. Fagotti, Dynamical Phase Transitions as Properties of the Stationary State: Analytic Results after Quantum Quenches in the Spin-1/2 XXZ Chain (2013), [arXiv:1308.0277](#).
- [35] S. Vajna and B. Dóra, Disentangling dynamical phase transitions from equilibrium phase transitions, *Physical Review B* **89**, 161105 (2014).
- [36] F. Andraschko and J. Sirker, Dynamical quantum phase transitions and the Loschmidt echo: A transfer matrix

- approach, *Physical Review B* **89**, 125120 (2014).
- [37] K. G. Wilson, Confinement of quarks, *Phys. Rev. D* **10**, 2445 (1974).
- [38] J. Kogut and L. Susskind, Hamiltonian formulation of Wilson's lattice gauge theories, *Physical Review D* **11**, 395 (1975).
- [39] J. Smit, *Introduction to Quantum Fields on a Lattice*, Cambridge Lecture Notes in Physics (Cambridge University Press, 2002) pp. 1–284.
- [40] D. Banerjee, M. Dalmonte, M. Müller, E. Rico, P. Stebler, U.-J. Wiese, and P. Zoller, Atomic Quantum Simulation of Dynamical Gauge Fields Coupled to Fermionic Matter: From String Breaking to Evolution after a Quench, *Physical Review Letters* **109**, 175302 (2012), [arXiv:arXiv:1205.6366v2](#).
- [41] S. Kühn, J. I. Cirac, and M. C. Bañuls, Quantum simulation of the Schwinger model: A study of feasibility, *Physical Review A - Atomic, Molecular, and Optical Physics* **90**, 1 (2014).
- [42] V. Kasper, F. Hebenstreit, M. Oberthaler, and J. Berges, Schwinger pair production with ultracold atoms, *Physics Letters B* **760**, 742 (2016).
- [43] A. S. Dehkharghani, E. Rico, N. T. Zinner, and A. Negretti, Quantum simulation of Abelian lattice gauge theories via state-dependent hopping, *Physical Review A* **96**, 043611 (2017).
- [44] A. Mil, T. V. Zache, A. Hegde, A. Xia, R. P. Bhatt, M. K. Oberthaler, P. Hauke, J. Berges, and F. Jendrzejewski, *Realizing a scalable building block of a U(1) gauge theory with cold atomic mixtures* (2019), [arXiv:1909.07641](#).
- [45] L. Sanchez-Palencia, Constructing Field Theories Using Quantum Simulators, *Physics* **13**, 10 (2020).
- [46] T. V. Zache, T. Schweigler, S. Erne, J. Schmiedmayer, and J. Berges, Extracting the Field Theory Description of a Quantum Many-Body System from Experimental Data, *Physical Review X* **10**, 011020 (2020), [arXiv:1909.12815](#).
- [47] B. Yang, H. Sun, R. Ott, H.-Y. Wang, T. V. Zache, J. C. Halimeh, Z.-S. Yuan, P. Hauke, and J.-W. Pan, *Observation of gauge invariance in a 71-site quantum simulator* (2020), [arXiv:2003.08945](#).
- [48] D. Horn, Finite matrix models with continuous local gauge invariance, *Physics Letters B* **100**, 149 (1981).
- [49] P. Orland and D. Rohrlich, Lattice gauge magnets: Local isospin from spin, *Nuclear Physics B* **338**, 647 (1990).
- [50] S. Chandrasekharan and U.-J. Wiese, Quantum link models: A discrete approach to gauge theories, *Nuclear Physics B* **492**, 455 (1997), [arXiv:9609042v2](#) [[arXiv:hep-lat](#)].
- [51] P. Hauke, D. Marcos, M. Dalmonte, and P. Zoller, Quantum Simulation of a Lattice Schwinger Model in a Chain of Trapped Ions, *Physical Review X* **3**, 041018 (2013), [arXiv:arXiv:1306.2162v3](#).
- [52] J. Preskill, Quantum Computing in the NISQ era and beyond, *Quantum* **2**, 79 (2018).
- [53] N. Bergeal, R. Vijay, V. E. Manucharyan, I. Siddiqi, R. J. Schoelkopf, S. M. Girvin, and M. H. Devoret, Analog information processing at the quantum limit with a Josephson ring modulator, *Nature Physics* **6**, 296 (2010).
- [54] M. Kounalakis, C. Dickel, A. Bruno, N. K. Langford, and G. A. Steele, Tuneable hopping and nonlinear cross-Kerr interactions in a high-coherence superconducting circuit, *npj Quantum Information* **4**, 38 (2018), [arXiv:1802.10037](#).
- [55] T. Roy, S. Kundu, M. Chand, S. Hazra, N. Nehra, R. Cosmic, A. Ranadive, M. P. Patankar, K. Damle, and R. Vijay, Implementation of Pairwise Longitudinal Coupling in a Three-Qubit Superconducting Circuit, *Physical Review Applied* **7**, 054025 (2017), [arXiv:1610.07915](#).
- [56] T. Roy, S. Hazra, S. Kundu, M. Chand, M. P. Patankar, and R. Vijay, A programmable three-qubit superconducting processor with all-to-all connectivity, [arXiv:1809.00668](#) (2018).
- [57] U. Vool and M. H. Devoret, Introduction to quantum electromagnetic circuits, *International Journal of Circuit Theory and Applications* **45**, 897 (2017), [arXiv:arXiv:1610.03438v2](#).
- [58] J. Schwinger, Gauge Invariance and Mass. II, *Phys. Rev.* **128**, 2425 (1962).
- [59] S. Coleman, R. Jackiw, and L. Susskind, Charge Shielding and Quark Confinement in the Massive Schwinger Model\*, *Annals of Physics* **275**, 267 (1975).
- [60] P. Jordan and E. Wigner, Über das Paulische Äquivalenzverbot, *Zeitschrift für Physik* **47**, 631 (1928).
- [61] L. Susskind, Lattice fermions, *Physical Review D* **16**, 3031 (1977).
- [62] D. Marcos, P. Rabl, E. Rico, and P. Zoller, Superconducting Circuits for Quantum Simulation of Dynamical Gauge Fields, *Physical Review Letters* **111**, 10.1103/PhysRevLett.111.110504 (2013), [arXiv:arXiv:1306.1674v2](#).
- [63] D. Marcos, P. Widmer, E. Rico, M. Hafezi, P. Rabl, U.-J. Wiese, and P. Zoller, Two-dimensional lattice gauge theories with superconducting quantum circuits, *Annals of Physics* **351**, 634 (2014), [arXiv:arXiv:1407.6066v2](#).
- [64] A. Mezzacapo, E. Rico, C. Sabín, I. L. Egusquiza, L. Lamata, and E. Solano, Non-Abelian SU(2) Lattice Gauge Theories in Superconducting Circuits, *Phys. Rev. Lett.* **115**, 240502 (2015), [arXiv:arXiv:1505.04720v2](#).
- [65] K. Le Hur, L. Henriet, A. Petrescu, K. Plekhanov, G. Roux, and M. Schiró, Many-body quantum electrodynamics networks: Non-equilibrium condensed matter physics with light, *Comptes Rendus Physique* **17**, 808 (2016).
- [66] M. J. Hartmann, Quantum simulation with interacting photons, *Journal of Optics* **18**, 104005 (2016).
- [67] G. K. Brennen, G. Pupillo, E. Rico, T. M. Stace, and D. Vodola, Loops and Strings in a Superconducting Lattice Gauge Simulator, *Physical Review Letters* **117**, 1 (2016), [arXiv:arXiv:1512.06565v2](#).
- [68] H. Alaeian, C. W. S. Chang, M. V. Moghaddam, C. M. Wilson, E. Solano, and E. Rico, *Lattice gauge fields via modulation in circuit QED: The bosonic Creutz ladder* (2018), [arXiv:1805.12410](#).
- [69] N. Klcio, E. F. Dumitrescu, A. J. McCaskey, T. D. Morris, R. C. Pooser, M. Sanz, E. Solano, P. Lougovski, and M. J. Savage, Quantum-classical computation of Schwinger model dynamics using quantum computers, *Physical Review A* **98**, 032331 (2018).
- [70] P. Roushan, C. Neill, A. Megrant, Y. Chen, R. Babush, R. Barends, B. Campbell, Z. Chen, B. Chiaro, A. Dunsworth, A. Fowler, E. Jeffrey, J. Kelly, E. Lucero, J. Mutus, P. J. O'Malley, M. Neeley, C. Quintana,



- D. Sank, A. Vainsencher, J. Wenner, T. White, E. Kapit, H. Neven, and J. M. Martinis, Chiral ground-state currents of interacting photons in a synthetic magnetic field, *Nature Physics* **13**, 146 (2017), [arXiv:arXiv:1606.00077v3](#).
- [71] Z. H. Yang, Y. P. Wang, Z. Y. Xue, W. L. Yang, Y. Hu, J. H. Gao, and Y. Wu, Circuit quantum electrodynamics simulator of flat band physics in a Lieb lattice, *Physical Review A* **93**, 1 (2016), [arXiv:arXiv:1603.04686v2](#).
- [72] M. A. Nielsen, A simple formula for the average gate fidelity of a quantum dynamical operation, *Physics Letters A* **303**, 249 (2002).
- [73] J. Koch, T. M. Yu, J. Gambetta, A. A. Houck, D. I. Schuster, J. Majer, A. Blais, M. H. Devoret, S. M. Girvin, and R. J. Schoelkopf, Charge-insensitive qubit design derived from the Cooper pair box, *Phys. Rev. A* **76**, 42319 (2007), [arXiv:0703002v2 \[arXiv:cond-mat\]](#).
- [74] A. Gyenis, P. S. Mundada, A. Di Paolo, T. M. Hazard, X. You, D. I. Schuster, J. Koch, A. Blais, and A. A. Houck, *Experimental realization of an intrinsically error-protected superconducting qubit* (2019), [arXiv:1910.07542](#).
- [75] M. Abuwasib, P. Krantz, and P. Delsing, Fabrication of large dimension aluminum air-bridges for superconducting quantum circuits, *Journal of Vacuum Science & Technology B, Nanotechnology and Microelectronics: Materials, Processing, Measurement, and Phenomena* **31**, 031601 (2013).
- [76] Z. Chen, A. Megrant, J. Kelly, R. Barends, J. Bochmann, Y. Chen, B. Chiaro, A. Dunsworth, E. Jeffrey, J. Y. Mutus, P. J. J. O'Malley, C. Neill, P. Roushan, D. Sank, A. Vainsencher, J. Wenner, T. C. White, A. N. Cleland, and J. M. Martinis, Fabrication and characterization of aluminum airbridges for superconducting microwave circuits, *Applied Physics Letters* **104**, 052602 (2014).
- [77] Z.-C. Jin, H.-T. Wu, H.-F. Yu, and Y. Yu, Fabrication of Al air-bridge on coplanar waveguide, *Chinese Physics B* **27**, 100310 (2018).
- [78] A. Dunsworth, R. Barends, Y. Chen, Z. Chen, B. Chiaro, A. Fowler, B. Foxen, E. Jeffrey, J. Kelly, P. V. Klimov, E. Lucero, J. Y. Mutus, M. Neeley, C. Neill, C. Quintana, P. Roushan, D. Sank, A. Vainsencher, J. Wenner, T. C. White, H. Neven, J. M. Martinis, and A. Megrant, A method for building low loss multi-layer wiring for superconducting microwave devices, *Applied Physics Letters* **112**, 063502 (2018).
- [79] H. Mukai, K. Sakata, S. J. Devitt, R. Wang, Y. Zhou, Y. Nakajima, and J. S. Tsai, *Pseudo-2D superconducting quantum computing circuit for the surface code: the proposal and preliminary tests* (2019), [arXiv:1902.07911](#).
- [80] V. Schmitt, *Design, fabrication and test of a four superconducting quantum-bit processor*, *Theses*, Université Pierre et Marie Curie - Paris VI (2015).
- [81] S. P. Pedersen, K. S. Christensen, and N. T. Zinner, Native three-body interaction in superconducting circuits, *Physical Review Research* **1**, 033123 (2019).
- [82] P. Krantz, M. Kjaergaard, F. Yan, T. P. Orlando, S. Gustavsson, and W. D. Oliver, *A Quantum Engineer's Guide to Superconducting Qubits* (2019), [arXiv:1904.06560](#).
- [83] M. A. Rol, F. Battistel, F. K. Malinowski, C. C. Bultink, B. M. Tarasinski, R. Vollmer, N. Haider, N. Muthusubramanian, A. Bruno, B. M. Terhal, and L. DiCarlo, Fast, High-Fidelity Conditional-Phase Gate Exploiting Leakage Interference in Weakly Anharmonic Superconducting Qubits, *Physical Review Letters* **123**, 120502 (2019).
- [84] P. Zhao, P. Xu, D. Lan, X. Tan, H. Yu, and Y. Yu, *High-contrast ZZ interaction using multi-type superconducting qubits* (2020), [arXiv:2002.07560](#).
- [85] N. J. S. Loft, M. Kjaergaard, L. B. Kristensen, C. K. Andersen, T. W. Larsen, S. Gustavsson, W. D. Oliver, and N. T. Zinner, *Quantum interference device for controlled two-qubit operations* (2018), [arXiv:1809.09049](#).
- [86] T. Bækkegaard, L. B. Kristensen, N. J. S. Loft, C. K. Andersen, D. Petrosyan, and N. T. Zinner, Realization of efficient quantum gates with a superconducting qubit-qutrit circuit, *Scientific Reports* **9**, 13389 (2019).
- [87] S. E. Rasmussen, K. S. Christensen, and N. T. Zinner, Controllable two-qubit swapping gate using superconducting circuits, *Physical Review B* **99**, 134508 (2019).
- [88] R. E. Barfknecht, S. E. Rasmussen, A. Foerster, and N. T. Zinner, Realizing time crystals in discrete quantum few-body systems, *Physical Review B* **99**, 144304 (2019).
- [89] Z. Wang, S. Shankar, Z. K. Mineev, P. Campagne-Ibarcq, A. Narla, and M. H. Devoret, Cavity Attenuators for Superconducting Qubits, *Phys. Rev. Applied* **11**, 14031 (2019).
- [90] S. Touzard, A. Kou, N. E. Frattini, V. V. Sivak, S. Puri, A. Grimm, L. Frunzio, S. Shankar, and M. H. Devoret, Gated Conditional Displacement Readout of Superconducting Qubits, *Phys. Rev. Lett.* **122**, 80502 (2019).
- [91] L. Qin, L. Xu, W. Feng, and X.-Q. Li, Qubit state tomography in a superconducting circuit via weak measurements, *New Journal of Physics* **19**, 033036 (2017).
- [92] M. Baur, A. Fedorov, L. Steffen, S. Filipp, M. P. da Silva, and A. Wallraff, Benchmarking a Quantum Teleportation Protocol in Superconducting Circuits Using Tomography and an Entanglement Witness, *Physical Review Letters* **108**, 040502 (2012).
- [93] S. Filipp, P. Maurer, P. J. Leek, M. Baur, R. Bianchetti, J. M. Fink, M. Göppl, L. Steffen, J. M. Gambetta, A. Blais, and A. Wallraff, Two-Qubit State Tomography Using a Joint Dispersive Readout, *Phys. Rev. Lett.* **102**, 200402 (2009).
- [94] L. Dicarlo, J. M. Chow, J. M. Gambetta, L. S. Bishop, B. R. Johnson, D. I. Schuster, J. Majer, A. Blais, L. Frunzio, S. M. Girvin, and R. J. Schoelkopf, Demonstration of two-qubit algorithms with a superconducting quantum processor, *Nature* **460**, 240 (2009), [arXiv:0903.2030](#).
- [95] M. Steffen, M. Ansmann, R. C. Bialczak, N. Katz, E. Lucero, R. McDermott, M. Neeley, E. M. Weig, a. N. Cleland, and J. M. Martinis, Measurement of the Entanglement of Two Superconducting Qubits via State Tomography, *Science* **313**, 1423 (2006).
- [96] A. J. Daley, H. Pichler, J. Schachenmayer, and P. Zoller, Measuring entanglement growth in quench dynamics of bosons in an optical lattice, *Physical Review Letters* **109**, 1 (2012), [arXiv:1205.1521](#).
- [97] H. Pichler, L. Bonnes, A. J. Daley, A. M. Läuchli, and P. Zoller, Thermal versus entanglement entropy: A measurement protocol for fermionic atoms with a quantum gas microscope, *New Journal of Physics* **15**, 10.1088/1367-2630/15/6/063003 (2013), [arXiv:1302.1187](#).

- [98] R. Islam, R. Ma, P. M. Preiss, M. E. Tai, A. Lukin, M. Rispoli, and M. Greiner, [Measuring entanglement entropy through the interference of quantum many-body twins](#) (2015), [arXiv:1509.01160](#).
- [99] N. M. Linke, S. Johri, C. Figgatt, K. A. Landsman, A. Y. Matsuura, and C. Monroe, Measuring the Rényi entropy of a two-site Fermi-Hubbard model on a trapped ion quantum computer, [Physical Review A](#) **98**, 052334 (2018).
- [100] T. Brydges, A. Elben, P. Jurcevic, B. Vermersch, C. Maier, B. P. Lanyon, P. Zoller, R. Blatt, and C. F. Roos, Probing Rényi entanglement entropy via randomized measurements, [Science](#) **364**, 260 (2019).
- [101] J. Heinsoo, C. K. Andersen, A. Remm, S. Krinner, T. Walter, Y. Salathé, S. Gasparinetti, J.-C. Besse, A. Poto, ifmmode \checkc\else c\finik, A. Wallraff, and C. Eichler, Rapid High-fidelity Multiplexed Readout of Superconducting Qubits, [Phys. Rev. Applied](#) **10**, 34040 (2018).
- [102] G. E. Fisher, *Lectures in Theoretical Physics*, Lectures in Theoretical Physics: Lectures Delivered at the Summer Institute for Theoretical Physics, University of Colorado, Boulder, Vol. 7 (University of Colorado Press, Boulder, 1965).
- [103] C. G. Callan, R. F. Dashen, and D. J. Gross, The structure of the gauge theory vacuum, [Physics Letters B](#) **63**, 334 (1976).
- [104] R. Jackiw and C. Rebbi, Vacuum periodicity in a Yang-Mills quantum theory, [Physical Review Letters](#) **37**, 172 (1976).
- [105] S. Coleman, More about the massive Schwinger model, [Annals of Physics](#) **101**, 239 (1976).
- [106] T. Schäfer and E. V. Shuryak, Instantons in QCD, [Reviews of Modern Physics](#) **70**, 323 (1998).
- [107] G. Gabadadze and M. Shifman, QCD vacuum and Axions: What's Happening?, [International Journal of Modern Physics A](#) **17**, 3689 (2002), [arXiv:0206123v1 \[arXiv:hep-ph\]](#).
- [108] R. D. Peccei, The strong CP problem and axions, [Lecture Notes in Physics](#) **741**, 3 (2008), [arXiv:0607268v1 \[arXiv:hep-ph\]](#).
- [109] R. D. Peccei, D. B. Tanner, and K. A. van Bibber, Why PQ?, [AIP Conference Proceedings](#) **1274**, 7 (2010).
- [110] J. E. Kim and G. Carosi, Axions and the strong CP problem, [Reviews of Modern Physics](#) **82**, 557 (2010), [arXiv:arXiv:0807.3125v2](#).
- [111] S. Pancharatnam, Generalized theory of interference and its applications, [Proceedings of the Indian Academy of Sciences - Section A](#) **44**, 398 (1956).
- [112] J. Samuel and R. Bhandari, General Setting for Berry's Phase, [Physical Review Letters](#) **60**, 2339 (1988).
- [113] T. Fukui, Y. Hatsugai, and H. Suzuki, Chern numbers in discretized Brillouin zone: Efficient method of computing (spin) Hall conductances, [Journal of the Physical Society of Japan](#) **74**, 1674 (2005).

## VII. ACKNOWLEDGEMENTS

The authors would like to thank Torsten Zache for insightful discussions. The authors would also like to thank K. S. Christensen, N. J. S. Loft, S. E. Rasmussen, L. B. Kristensen and T. Bækkegaard for general discussions pertaining to this work. The authors acknowledge support from the Independent Research Fund Denmark, the Carlsberg Foundation, and AUFF through the Jens Chr. Skou fellowship program.

## VIII. AUTHOR CONTRIBUTIONS

S.P.P. and N.T.Z. proposed the system, designed the study and methods. S.P.P. conducted the simulations and analysed the results. S.P.P. wrote the initial draft of the manuscript. S.P.P. and N.T.Z. contributed to the editing towards the final version for publication.

## IX. COMPETING INTERESTS

The authors declare no competing interests.

## X. ADDITIONAL INFORMATION

**Supplementary information** is available for this paper at

**Correspondence** and requests for materials should be addressed to S.P.P.

# Supplemental Information: Lattice gauge theory and dynamical quantum phase transitions using noisy intermediate scale quantum devices

Simon Panyella Pedersen\*

*Department of Physics and Astronomy, Aarhus University, DK-8000 Aarhus C, Denmark*

N. T. Zinner†

*Department of Physics and Astronomy, Aarhus University, DK-8000 Aarhus C, Denmark and  
Aarhus Institute of Advanced Studies, Aarhus University, DK-8000 Aarhus C, Denmark*

(Dated: October 6, 2021)

## SUPPLEMENTARY METHODS

In the five sections below we give additional details on the following: First a full derivation of the Hamiltonian, anharmonicities and further details of our proposed circuit, using a method for truncation devised by the authors that does not implement a Taylor expansion, yielding more exact spin model parameters. Secondly, we briefly detail how we numerically found the necessary effective spin model parameters, which take renormalization from interactions with levels outside the spin-1/2 subspace in account. Thirdly, we discuss how circuit parameters are optimized to yield appropriate spin model parameters, anharmonicities, and a good fidelity for the desired dynamics. Fourthly, we briefly derive the time evolution operator in a rotating frame. Finally, we detail how the average fidelity is calculated, and how it is to be interpreted.

### A. Deriving the circuit Hamiltonian

In a superconducting circuit of transmon qubits there is natively two-body interactions, as an interaction is between nodes and is mediated by a branch, which could of course never connect more than two nodes at a time. To get multi-body interactions we therefore need to change coordinates. Below we change coordinates to the eigenmodes of the capacitance network, which simultaneously removes all interactions from capacitors (making the system simpler), and allows for multi-body interactions, in particular the three-body XXX-coupling, we are interested in. The intuition is that these modes are more spread out on the circuit and so more than two at a time can "be at the same place" and interact. In particular multi-body interactions come from Josephson junctions terms, as these are non-linear. Capacitance and linear inductive terms are square in the coordinates, and so could never couple more than two at a time.

The only way (seemingly) to get a direct, triple, odd (i.e. originates from a product of creation/annihilation operators which all have an odd power) interaction like the XXX-coupling using capacitors, linear inductors, and Josephson junctions in a superconducting circuit, is to shift the position of the minimum of the potential away from the origin. Otherwise, all circuit elements contribute with terms that are even in the number of flux coordinates. This shifting is done by introducing (constant) drives of the potential terms, such that the different functions and their minima are shifted relative to each other. Shifting the minimum and expanding around it makes no difference for capacitive and linear inductive terms. Capacitive terms involve the derivative and so do not care about a constant shift, while linear inductive terms can only give first and second order terms (in the fluxes), and all first order terms disappear when we expand around an extremal point, like the potential minimum. Hence, we only get new and interesting terms from the Josephson junction. This in turn give us a myriad of messy terms. Consider the following cosine term, in the context of a larger system, where the coordinates are chosen such that the minimum of the full potential is at the origin,  $\phi = 0$ , but such that the argument of the cosine is shifted

$$\cos(\phi + \alpha) = \cos(\alpha) - \sin(\alpha)\phi - \frac{1}{2}\cos(\alpha)\phi^2 + \frac{1}{6}\sin(\alpha)\phi^3 + \frac{1}{24}\cos(\alpha)\phi^4 + \mathcal{O}(\phi^5)$$

---

\* spp@phys.au.dk

† zinner@phys.au.dk

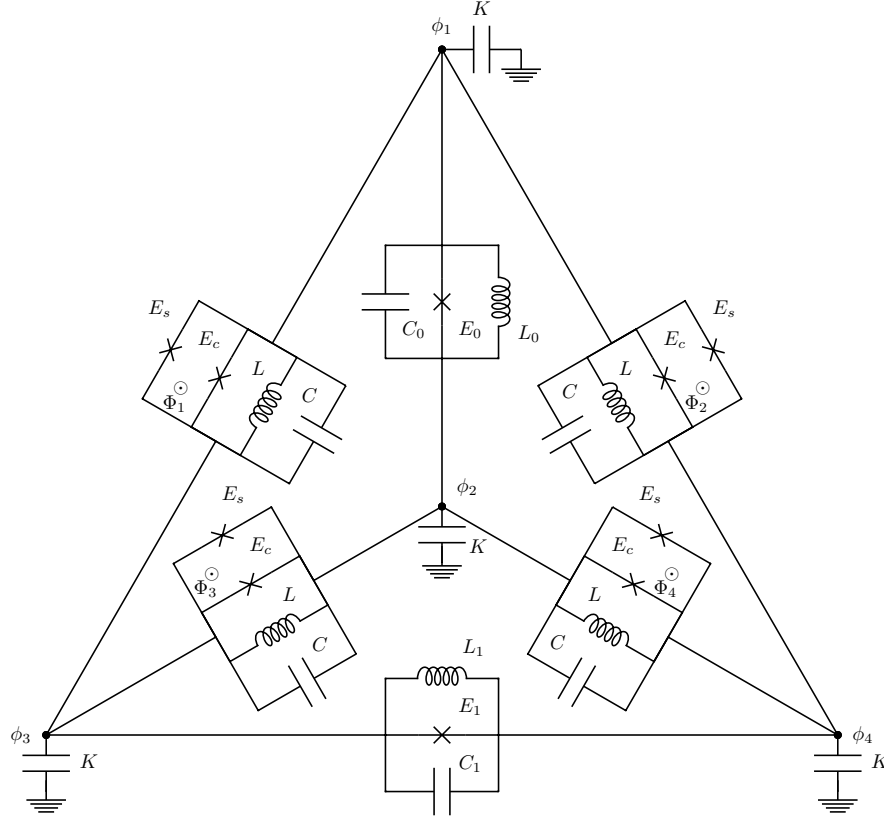


Figure 1. The circuit for implementing the XXX-coupling in a more general form than the used in the main text. We have here included linear inductors on all branches for the sake of generality.

Here  $\phi$  represents any combination of fluxes and  $\alpha$  is a shift combining different (constant) drives in the cosine, and shifts of the coordinates/potential. We are interested in the  $\phi^3$  term for our XXX interaction. We seek a circuit whose symmetry ensures that all the undesired terms cancel. As we seek a three-body interaction we will work with a circuit of four nodes, all-to-all connected, and in the basis of the eigenvectors of the capacitance matrix, i.e. the eigenmodes of the capacitive network. Working in this basis removes interactions from capacitors, reducing the complexity by a lot, and also allows for more than two coordinates to be involved in the same term, yielding multi-body interactions.

In Fig. 1 can be seen our circuit in a more general form than was used in the main text. We have here included linear inductors on all branches for the sake of studying the most general case of the circuit. Notice the symmetry of the circuit parameters. Defining the original node flux coordinates  $\vec{\phi} = (\phi_1, \phi_2, \phi_3, \phi_4)$ , the circuit has the following capacitance matrix

$$\mathcal{C} = \begin{pmatrix} 2C + C_0 + K & -C_0 & -C & -C \\ -C_0 & 2C + C_0 + K & -C & -C \\ -C & -C & 2C + C_1 + K & -C_1 \\ -C & -C & -C_1 & 2C + C_1 + K \end{pmatrix}$$

We define new coordinates  $\vec{\psi} = (\psi_{CM}, \psi_1, \psi_g, \psi_2)$ , and make a change of coordinates according to

$$\vec{\phi} = \begin{pmatrix} 1 & 1 & \frac{1}{2} & 0 \\ 1 & -1 & \frac{1}{2} & 0 \\ 1 & 0 & -\frac{1}{2} & 1 \\ 1 & 0 & -\frac{1}{2} & -1 \end{pmatrix} \vec{\psi}$$

Notice that the coordinates  $\psi_1$  and  $\psi_2$  are simply  $\phi_2 - \phi_3$  and  $\phi_1 - \phi_4$ , making the terms corresponding to these branches affect only these modes individually, while  $\phi_g$  will be affected by the four branches with identical circuit

parameters. This transformation diagonalizes the capacitance matrix to

$$\mathcal{K} = \begin{pmatrix} 4K & 0 & 0 & 0 \\ 0 & 4C + 4C_0 + 2K & 0 & 0 \\ 0 & 0 & 4C + K & 0 \\ 0 & 0 & 0 & 4C + 4C_1 + 2K \end{pmatrix}$$

It is important here that the capacitance to ground is identical for all nodes, as it will otherwise introduce interactions.

Now let us consider the Josephson junctions on the branches pertaining to the  $\psi_g$  mode. Taking either of the four junctions with subscript  $c$  or  $s$ , we find that they can be neatly summed as follows

$$\begin{aligned} & \cos(\phi_1 - \phi_2) + \cos(\phi_1 - \phi_3) + \cos(\phi_2 - \phi_4) + \cos(\phi_3 - \phi_4) \\ &= \cos(-\psi_1 + \psi_g + \psi_2) + \cos(\psi_1 + \psi_g + \psi_2) + \cos(\psi_1 - \psi_g + \psi_2) + \cos(-\psi_1 - \psi_g + \psi_2) \\ &= 2 \cos(\psi_1) \cos(\psi_g + \psi_2) + 2 \cos(\psi_1) \cos(\psi_g - \psi_2) \\ &= 4 \cos(\psi_1) \cos(\psi_g) \cos(\psi_2) \end{aligned}$$

Hence, these four junctions result in some very neat interactions between the modes and contributions to their energies and anharmonicities. We choose the spanning tree and the exact layout of the circuit such that the external fluxes,  $\Phi_i$ ,  $i = 1, 2, 3, 4$ , enter in the junctions with subscript  $s$ . We then choose the  $\Phi_i$ 's as sums of three other fluxes  $\Psi_j$ ,  $j = 1, g, 2$ , where the sign of each  $\Psi_j$  in each cosine term must be the same as the corresponding  $\psi_j$ . For example, if we include  $\Phi_1$  in the first cosine in the above calculation,  $\cos(\phi_1 - \phi_2 + \Phi_1) = \cos(-\psi_1 + \psi_g + \psi_2 + \Phi_1)$ , then we can see that choosing  $\Phi_1 = -\Psi_1 + \Psi_g + \Psi_2$  results in a  $\Psi_j$ -term for each  $\psi_j$  with the same sign. Doing the same with all four cosines, we essentially shift  $\psi_j \rightarrow \psi_j + \Psi_j$ . The result of the above calculation would then be

$$4 \cos(\psi_1 + \Psi_1) \cos(\psi_g + \Psi_g) \cos(\psi_2 + \Psi_2)$$

Hence, we can use these to tune the interactions pertaining to  $E_s$ . In particular choosing  $\Psi_j = -\frac{\pi}{2}$  for all  $j$ , we get a triple sine interaction. The triple sine will have its minimum at  $\psi_j = 0$ , as all other terms already did, and so this shift will only affect this particular term of the Hamiltonian. Expanding to fourth order, it yields exactly a  $\psi_1 \psi_g \psi_2$  interaction corresponding to the desired XXX coupling. Likewise for the four linear inductors we find

$$\begin{aligned} & (\phi_1 - \phi_2)^2 + (\phi_1 - \phi_3)^2 + (\phi_2 - \phi_4)^2 + (\phi_3 - \phi_4)^2 \\ &= (-\psi_1 + \psi_g + \psi_2)^2 + (\psi_1 + \psi_g + \psi_2)^2 + (\psi_1 - \psi_g + \psi_2)^2 + (-\psi_1 - \psi_g + \psi_2)^2 \\ &= 4(\psi_1^2 + \psi_g^2 + \psi_2^2) \end{aligned}$$

Thus they do not introduce any interaction, as mentioned above, but merely add to the harmonicity and energy of the modes. The cosines pertaining to  $E_c$  will yield ZZ interaction, which we would rather be without, but they alone contribute to  $\psi_g$ 's anharmonicity. If we instead had only the identical linear inductors, we would get similar contributions to the mode energies, but no interactions and also no contribution to anharmonicities. In this case  $\psi_g$  would be a pure harmonic oscillator, but we would have fewer interactions. The other two modes get their anharmonicities from the  $E_1$  and  $E_2$  junctions. The inductors turn out to not be necessary but could be used to tune the energies of  $\psi_1$  and  $\psi_2$  if needed. In order for the XXX interaction to work the modes need to be detuned in a proper way, as described below.

With these calculations and in these coordinates, the Hamiltonian of the circuit becomes

$$\begin{aligned} H = & \frac{1}{2} \frac{1}{4C + 4C_1 + 2K} p_1^2 + \frac{1}{2} \frac{1}{4C + K} p_2^2 + \frac{1}{2} \frac{1}{4C + 4C_2 + 2K} p_2^2 \\ & + (4E_{L_1} + 4E_L) \psi_1^2 - E_1 \cos(2\psi_1) + 4E_L \psi_g^2 + (4E_{L_2} + 4E_L) \psi_2^2 - E_2 \cos(2\psi_2) \\ & - 4E_c \cos \psi_1 \cos \psi_g \cos \psi_2 \\ & - 4E_s \sin \psi_1 \sin \psi_g \sin \psi_2 \end{aligned}$$

where  $E_L = \frac{1}{2L}$  and likewise for the others. We will not be performing the usual expansion to fourth order before recasting and truncation, but will rather use a method developed by the author for in a previous paper [1], with which the trigonometric functions can be truncated without performing any approximation. To do so we perform the recasting in terms of harmonic oscillator modes first. We introduce bosonic creation and annihilation operators,  $a_j^\dagger, a_j$ , via

$$\begin{aligned} \psi_j &= \frac{r_j}{\sqrt{2}} (a_j^\dagger + a_j) \\ p_j &= i \frac{1}{\sqrt{2}r_j} (a_j^\dagger - a_j) \end{aligned}$$



Here  $r_j$  is parameter which quantifies the "size" of the  $\psi_j$  coordinate. When performing the usual expansion to fourth order, one is in fact expanding to fourth order in  $r_j/\sqrt{2}$ , and so the usual transmon regime (of circuit parameters) is when  $r_j/\sqrt{2}$  is very small. The  $r_j$  are defined as

$$r_j = \left( \frac{K_{p_j}}{K_{\psi_j}} \right)^{1/4}$$

where  $K_{p_j}$  and  $K_{\psi_j}$  are the coefficients of the  $p_j^2$  and the  $\psi_j^2$  terms, respectively, in the Hamiltonian, when it is expanded in powers of  $\psi_j$ . If we expand  $H$  to just second order to find these terms, we get

$$\begin{aligned} H &= \frac{1}{2} \frac{1}{4C + 4C_1 + 2K} p_1^2 + \frac{1}{2} \frac{1}{4C + K} p_2^2 + \frac{1}{2} \frac{1}{4C + 4C_2 + 2K} p_2^2 \\ &\quad + (4E_{L_1} + 4E_L) \psi_1^2 - E_1 (1 + 2\psi_1^2) + 4E_L \psi_g^2 + (4E_{L_2} + 4E_L) \psi_2^2 - E_2 (1 + 2\psi_2^2) \\ &\quad - 4E_c \left( 1 + \frac{1}{2} \psi_1^2 \right) \left( 1 + \frac{1}{2} \psi_g^2 \right) \left( 1 + \frac{1}{2} \psi_2^2 \right) \\ &\quad - 4E_s \psi_1 \psi_g \psi_2 + \mathcal{O}(\psi_j^3) \\ &= \frac{1}{2} \frac{1}{4C + 4C_1 + 2K} p_1^2 + \frac{1}{2} \frac{1}{4C + K} p_2^2 + \frac{1}{2} \frac{1}{4C + 4C_2 + 2K} p_2^2 \\ &\quad + (4E_{L_1} + 4E_L - 2E_1 - 2E_c) \psi_1^2 + (4E_L - 2E_c) \psi_g^2 + (4E_{L_2} + 4E_L - 2E_2 - 2E_c) \psi_2^2 + \mathcal{O}(\psi_j^3) \end{aligned}$$

where we have ignored constant terms and all terms involving more than two  $\psi_j$  are hidden in  $\mathcal{O}(\psi_j^3)$ . From this we can see that for example

$$\begin{aligned} K_{p_1} &= \frac{1}{2} \frac{1}{4C + 4C_1 + 2K} \\ K_{\phi_1} &= 4E_{L_1} + 4E_L - 2E_1 - 2E_c \end{aligned}$$

and similarly for the other coordinates. With these we can define

$$\begin{aligned} r_1 &= [8(2C + 2C_1 + K)(2E_{L_1} + 2E_L + E_1 + E_c)]^{-1/4} \\ r_g &= [4(4C + K)(2E_L + E_c)]^{-1/4} \\ r_2 &= [8(2C + 2C_2 + K)(2E_{L_2} + 2E_L + E_2 + E_c)]^{-1/4} \end{aligned}$$

We will be writing the trigonometric functions in terms of complex exponentials, as this helps us truncate them later on. Thus, we can write the Hamiltonian in terms of the creation and annihilation operators as

$$\begin{aligned} H &= -\frac{1}{2} \frac{1}{4C + 4C_1 + 2K} \frac{1}{2r_1^2} (a_1^\dagger - a_1)^2 - \frac{1}{2} \frac{1}{4C + K} \frac{1}{2r_g^2} (a_g^\dagger - a_g)^2 - \frac{1}{2} \frac{1}{4C + 4C_2 + 2K} \frac{1}{2r_2^2} (a_2^\dagger - a_2)^2 \\ &\quad + 4(E_{L_1} + E_L) \frac{r_1^2}{2} (a_1^\dagger + a_1)^2 - E_1 \frac{1}{2} \left( e^{i\sqrt{2}r_1(a_1^\dagger + a_1)} + e^{-i\sqrt{2}r_1(a_1^\dagger + a_1)} \right) \\ &\quad + 4E_L \frac{r_g^2}{2} (a_g^\dagger + a_g)^2 \\ &\quad + 4(E_{L_2} + E_L) \frac{r_2^2}{2} (a_2^\dagger + a_2)^2 - E_2 \frac{1}{2} \left( e^{i\sqrt{2}r_2(a_2^\dagger + a_2)} + e^{-i\sqrt{2}r_2(a_2^\dagger + a_2)} \right) \\ &\quad - \frac{1}{2} E_c \left( e^{ir_1(a_1^\dagger + a_1)/\sqrt{2}} + e^{-ir_1(a_1^\dagger + a_1)/\sqrt{2}} \right) \left( e^{ir_g(a_g^\dagger + a_g)/\sqrt{2}} + e^{-ir_g(a_g^\dagger + a_g)/\sqrt{2}} \right) \left( e^{ir_2(a_2^\dagger + a_2)/\sqrt{2}} + e^{-ir_2(a_2^\dagger + a_2)/\sqrt{2}} \right) \\ &\quad - \frac{i}{2} E_s \left( e^{ir_1(a_1^\dagger + a_1)/\sqrt{2}} - e^{-ir_1(a_1^\dagger + a_1)/\sqrt{2}} \right) \left( e^{ir_g(a_g^\dagger + a_g)/\sqrt{2}} - e^{-ir_g(a_g^\dagger + a_g)/\sqrt{2}} \right) \left( e^{ir_2(a_2^\dagger + a_2)/\sqrt{2}} - e^{-ir_2(a_2^\dagger + a_2)/\sqrt{2}} \right) \end{aligned}$$

In order to truncate this Hamiltonian to any number of desired levels in each mode, we must calculate the corresponding matrix elements of each operator in the Hamiltonian. The matrix elements are calculated in the Fock basis, and so operators like  $(a_j^\dagger \pm a_j)^2$  are easily dealt with. Indeed, it is the trigonometric functions, now in terms of exponentials, that require some work. Here we recognize that the exponentials are on the form of a displacement operator, known from harmonic oscillators,

$$D(\xi) = e^{\xi a^\dagger - \xi^* a}$$

Here  $\xi$  is some complex number, and the fundamental property of the displacement operator is that  $D(\xi)|0\rangle = |\xi\rangle$ , where  $|0\rangle$  is the ground state of the harmonic oscillator,  $a|0\rangle = 0$ , and  $|\xi\rangle$  is a coherent state. The coherent states can in turn be written out as a series, specifically

$$D(\xi)|0\rangle = e^{-|\xi|^2/2} \sum_{j=0}^{\infty} \frac{\xi^j}{\sqrt{j!}} |j\rangle$$

Furthermore, we know the commutations relations of the displacement operator

$$D(\xi)a^\dagger = (a^\dagger - \xi^*)D(\xi)$$

With these relations and the definition  $|n\rangle = \frac{1}{\sqrt{n!}}(a^\dagger)^n|0\rangle$ , we can calculate the needed matrix elements. Looking at the Hamiltonian we see that we will only need to consider  $\xi = ik$  for some real number  $k$ . Let us therefore consider the general case, and find the matrix elements of  $D(ik) = e^{ik(a^\dagger+a)}$ . Let us also note that since the operator  $a^\dagger + a$  is symmetric, the operator  $D(ik) = e^{ik(a^\dagger+a)}$  is also symmetric, i.e.  $\langle n|e^{ik(a^\dagger+a)}|m\rangle = \langle m|e^{ik(a^\dagger+a)}|n\rangle$ . We find with the above relations

$$\begin{aligned}\langle 0|e^{ik(a^\dagger+a)}|0\rangle &= e^{-k^2/2} \\ \langle 1|e^{ik(a^\dagger+a)}|0\rangle &= ik e^{-k^2/2} \\ \langle 1|e^{ik(a^\dagger+a)}|1\rangle &= (1 - k^2)e^{-k^2/2}\end{aligned}$$

With these we can write the operator  $e^{ik(a^\dagger+a)}$  truncated to two levels in terms of Pauli matrices and the identity

$$M_2 \left[ e^{ik(a^\dagger+a)} \right] = \left[ \left( 1 - \frac{k^2}{2} \right) + \frac{k^2}{2} \sigma^z + ik \sigma^x \right] e^{-k^2/2}$$

where  $M_n[\cdot]$  is the  $n \times n$  matrix representation of an operator. It is now just a matter of replacing exponentials with this expression and reducing the result, i.e. we don't need to perform the truncation calculation more than once, from now on it is just a mechanical method of inserting the right expressions into our equations. Likewise we can find the following standard two-level expressions for the remaining operators

$$\begin{aligned}M_2[a^\dagger a] &= \frac{1}{2} (1 - \sigma^z) \\ M_2[a^\dagger - a] &= -i\sigma^y \\ M_2[(a^\dagger - a)^2] &= -2 + \sigma^z \\ M_2[a^\dagger + a] &= \sigma^x \\ M_2[(a^\dagger + a)^2] &= 2 - \sigma^z\end{aligned}$$

This procedure is easily expanded to include more levels in the truncation. Performing this exact truncation of the trigonometric functions can reduce the numerical difficulty of simulating the dynamics of a circuit while including higher levels. Such a study is often relevant to check the actual effect of the higher levels of a circuit rather than only studying the approximate dynamics of system truncated to two levels in each mode.

We can thus calculate the two level Hamiltonian exactly. We do so

$$\begin{aligned}
H = & \frac{1}{2} \frac{1}{4C + 4C_1 + 2K} p_1^2 + \frac{1}{2} \frac{1}{4C + K} p_2^2 + \frac{1}{2} \frac{1}{4C + 4C_2 + 2K} p_2^2 \\
& + \left( \frac{2}{L_1} + \frac{2}{L} \right) \psi_1^2 - E_1 \cos(2\psi_1) + \frac{2}{L} \psi_g^2 + \left( \frac{2}{L_2} + \frac{2}{L} \right) \psi_2^2 - E_2 \cos(2\psi_2) \\
& - 4E_c \cos \psi_1 \cos \psi_g \cos \psi_2 \\
& - 4E_s \sin \psi_1 \sin \psi_g \sin \psi_2 \\
= & -\frac{1}{2} \frac{1}{4C + 4C_1 + 2K} \frac{1}{2r_1^2} (a_1^\dagger - a_1)^2 - \frac{1}{2} \frac{1}{4C + K} \frac{1}{2r_g^2} (a_g^\dagger - a_g)^2 - \frac{1}{2} \frac{1}{4C + 4C_2 + 2K} \frac{1}{2r_2^2} (a_2^\dagger - a_2)^2 \\
& + 4(E_{L_1} + E_L) \frac{r_1^2}{2} (a_1^\dagger + a_1)^2 - E_1 \frac{1}{2} \left( e^{i\sqrt{2}r_1(a_1^\dagger + a_1)} + e^{-i\sqrt{2}r_1(a_1^\dagger + a_1)} \right) \\
& + 4E_L \frac{r_g^2}{2} (a_g^\dagger + a_g)^2 \\
& + 4(E_{L_2} + E_L) \frac{r_2^2}{2} (a_2^\dagger + a_2)^2 - E_2 \frac{1}{2} \left( e^{i\sqrt{2}r_2(a_2^\dagger + a_2)} + e^{-i\sqrt{2}r_2(a_2^\dagger + a_2)} \right) \\
& - \frac{1}{2} E_c \left( e^{ir_1(a_1^\dagger + a_1)/\sqrt{2}} + e^{-ir_1(a_1^\dagger + a_1)/\sqrt{2}} \right) \left( e^{ir_g(a_g^\dagger + a_g)/\sqrt{2}} + e^{-ir_g(a_g^\dagger + a_g)/\sqrt{2}} \right) \left( e^{ir_2(a_2^\dagger + a_2)/\sqrt{2}} + e^{-ir_2(a_2^\dagger + a_2)/\sqrt{2}} \right) \\
& - \frac{i}{2} E_s \left( e^{ir_1(a_1^\dagger + a_1)/\sqrt{2}} - e^{-ir_1(a_1^\dagger + a_1)/\sqrt{2}} \right) \left( e^{ir_g(a_g^\dagger + a_g)/\sqrt{2}} - e^{-ir_g(a_g^\dagger + a_g)/\sqrt{2}} \right) \left( e^{ir_2(a_2^\dagger + a_2)/\sqrt{2}} - e^{-ir_2(a_2^\dagger + a_2)/\sqrt{2}} \right) \\
= & \frac{1}{2} \frac{1}{4C + 4C_1 + 2K} \frac{1}{2r_1^2} (2 - \sigma_1^z) + \frac{1}{2} \frac{1}{4C + K} \frac{1}{2r_g^2} (2 - \sigma_g^z) + \frac{1}{2} \frac{1}{4C + 4C_2 + 2K} \frac{1}{2r_2^2} (2 - \sigma_2^z) \\
& + 2(E_{L_1} + E_L) r_1^2 (2 - \sigma_1^z) - E_1 \left[ (1 - r_1^2) + r_1^2 \sigma_1^z \right] e^{-r_1^2} \\
& + 4E_L \frac{r_g^2}{2} (2 - \sigma_g^z) \\
& + 2(E_{L_2} + E_L) r_2^2 (2 - \sigma_2^z) - E_2 \left[ (1 - r_2^2) + r_2^2 \sigma_2^z \right] e^{-r_2^2} \\
& - \frac{1}{2} E_c \left[ \left( 2 - \frac{r_1^2}{2} \right) + \frac{r_1^2}{2} \sigma_1^z \right] \left[ \left( 2 - \frac{r_g^2}{2} \right) + \frac{r_g^2}{2} \sigma_g^z \right] \left[ \left( 2 - \frac{r_2^2}{2} \right) + \frac{r_2^2}{2} \sigma_2^z \right] e^{-(r_1^2 + r_g^2 + r_2^2)/4} \\
& - \frac{i}{2} E_s [\sqrt{2}ir_1\sigma_1^x][\sqrt{2}ir_g\sigma_g^x][\sqrt{2}ir_2\sigma_2^x] e^{-(r_1^2 + r_g^2 + r_2^2)/4} \\
= & -\frac{1}{2} \left[ 2(E_1 + 4E_{L_1} + 4E_L + E_c) r_1^2 + 2E_1 r_1^2 e^{-r_1^2} + \frac{E_c r_1^2}{2} \left( 2 - \frac{r_g^2}{2} \right) \left( 2 - \frac{r_2^2}{2} \right) e^{-\frac{r_1^2 + r_g^2 + r_2^2}{4}} \right] \sigma_1^z \\
& - \frac{1}{2} \left[ 2(4E_L + E_c) r_g^2 + \frac{E_c r_g^2}{2} \left( 2 - \frac{r_1^2}{2} \right) \left( 2 - \frac{r_2^2}{2} \right) e^{-\frac{r_1^2 + r_g^2 + r_2^2}{4}} \right] \sigma_g^z \\
& - \frac{1}{2} \left[ 2(E_2 + 4E_{L_2} + 4E_L + E_c) r_2^2 + 2E_2 r_2^2 e^{-r_2^2} + \frac{E_c r_2^2}{2} \left( 2 - \frac{r_1^2}{2} \right) \left( 2 - \frac{r_g^2}{2} \right) e^{-\frac{r_1^2 + r_g^2 + r_2^2}{4}} \right] \sigma_2^z \\
& - \frac{E_c r_1^2 r_g^2}{8} \left( 2 - \frac{r_2^2}{2} \right) e^{-\frac{r_1^2 + r_g^2 + r_2^2}{4}} \sigma_1^z \sigma_g^z \\
& - \frac{E_c r_1^2 r_2^2}{8} \left( 2 - \frac{r_g^2}{2} \right) e^{-\frac{r_1^2 + r_g^2 + r_2^2}{4}} \sigma_1^z \sigma_2^z \\
& - \frac{E_c r_g^2 r_2^2}{8} \left( 2 - \frac{r_1^2}{2} \right) e^{-\frac{r_1^2 + r_g^2 + r_2^2}{4}} \sigma_g^z \sigma_2^z \\
& - \frac{E_c r_1^2 r_g^2 r_2^2}{16} e^{-\frac{r_1^2 + r_g^2 + r_2^2}{4}} \sigma_1^z \sigma_g^z \sigma_2^z \\
& - \sqrt{2} E_s r_1 r_g r_2 e^{-\frac{r_1^2 + r_g^2 + r_2^2}{4}} \sigma_1^x \sigma_g^x \sigma_2^x
\end{aligned}$$

Defining the spin-model parameters

$$\begin{aligned}
\Omega_1 &= 2(E_1 + 4E_{L_1} + 4E_L + E_c)r_1^2 + 2E_1r_1^2e^{-r_1^2} \\
&\quad + \frac{E_cr_1^2}{2} \left(2 - \frac{r_g^2}{2}\right) \left(2 - \frac{r_2^2}{2}\right) e^{-\frac{r_1^2+r_g^2+r_2^2}{4}} \\
\Omega_g &= 2(4E_L + E_c)r_g^2 + \frac{E_cr_g^2}{2} \left(2 - \frac{r_1^2}{2}\right) \left(2 - \frac{r_2^2}{2}\right) e^{-\frac{r_1^2+r_g^2+r_2^2}{4}} \\
\Omega_2 &= 2(E_2 + 4E_{L_2} + 4E_L + E_c)r_2^2 + 2E_2r_2^2e^{-r_2^2} \\
&\quad + \frac{E_cr_2^2}{2} \left(2 - \frac{r_1^2}{2}\right) \left(2 - \frac{r_g^2}{2}\right) e^{-\frac{r_1^2+r_g^2+r_2^2}{4}} \\
J_{1g}^z &= -\frac{E_cr_1^2r_g^2}{8} \left(2 - \frac{r_2^2}{2}\right) e^{-\frac{r_1^2+r_g^2+r_2^2}{4}} \\
J_{12}^z &= -\frac{E_cr_1^2r_2^2}{8} \left(2 - \frac{r_g^2}{2}\right) e^{-\frac{r_1^2+r_g^2+r_2^2}{4}} \\
J_{g2}^z &= -\frac{E_cr_g^2r_2^2}{8} \left(2 - \frac{r_1^2}{2}\right) e^{-\frac{r_1^2+r_g^2+r_2^2}{4}} \\
J_{1g2}^z &= -\frac{E_cr_1^2r_g^2r_2^2}{16} e^{-\frac{r_1^2+r_g^2+r_2^2}{4}} \\
J_{1g2}^x &= -\sqrt{2}E_sr_1r_g r_2 e^{-\frac{r_1^2+r_g^2+r_2^2}{4}}
\end{aligned}$$

we get the final Hamiltonian

$$\begin{aligned}
H &= -\frac{1}{2}\Omega_1\sigma_1^z - \frac{1}{2}\Omega_g\sigma_g^z - \frac{1}{2}\Omega_2\sigma_2^z \\
&\quad + J_{1g}^z\sigma_1^z\sigma_g^z + J_{12}^z\sigma_1^z\sigma_2^z + J_{g2}^z\sigma_g^z\sigma_2^z \\
&\quad + J_{1g2}^z\sigma_1^z\sigma_g^z\sigma_2^z + J_{1g2}^x\sigma_1^x\sigma_g^x\sigma_2^x
\end{aligned}$$

Furthermore, the anharmonicities can be calculated with the same exact method, by including a third level and defining the anharmonicities as  $\alpha = E_{12} - E_{01}$ , where  $E_{ij}$  is the energy gap between level  $i$  and  $j$ , and the energies are defined as the diagonal entries of the Hamiltonian. With this we get the following anharmonicities

$$\begin{aligned}
\alpha_1 &= -2E_1r_1^4e^{-r_1^2} - \frac{E_cr_1^4}{2} \left(1 - \frac{r_g^2}{4}\right) \left(1 - \frac{r_2^2}{4}\right) e^{-\frac{r_1^2+r_g^2+r_2^2}{4}}, \\
\alpha_g &= -\frac{E_cr_g^4}{2} \left(1 - \frac{r_1^2}{4}\right) \left(1 - \frac{r_2^2}{4}\right) e^{-\frac{r_1^2+r_g^2+r_2^2}{4}}, \\
\alpha_2 &= -2E_2r_2^4e^{-r_2^2} - \frac{E_cr_2^4}{2} \left(1 - \frac{r_1^2}{4}\right) \left(1 - \frac{r_g^2}{4}\right) e^{-\frac{r_1^2+r_g^2+r_2^2}{4}}
\end{aligned}$$

In the main text we did not include the linear inductors in the circuit. Removing them corresponds simply to setting  $E_L, E_{L_0}, E_{L_1} = 0$  in the above expressions.

## B. Derive effective parameters

In the above section we found exact spin model parameters, taking two levels in each mode into account. For the detuning and XXX-coupling strength, however, we need to numerically find effective parameters, as the above bare spin model parameters are renormalized by virtual processes involving the higher levels of the system. We consider only the effective detuning and XXX-coupling strength this way, because they need to be accurate in order for the circuit to result in the desired dynamics, while anharmonicities and other parameters do not have such exact demands imposed on them. The effective detuning we are looking for is the detuning between the states  $|1_01_g0_1\rangle$  and  $|0_00_g1_1\rangle$

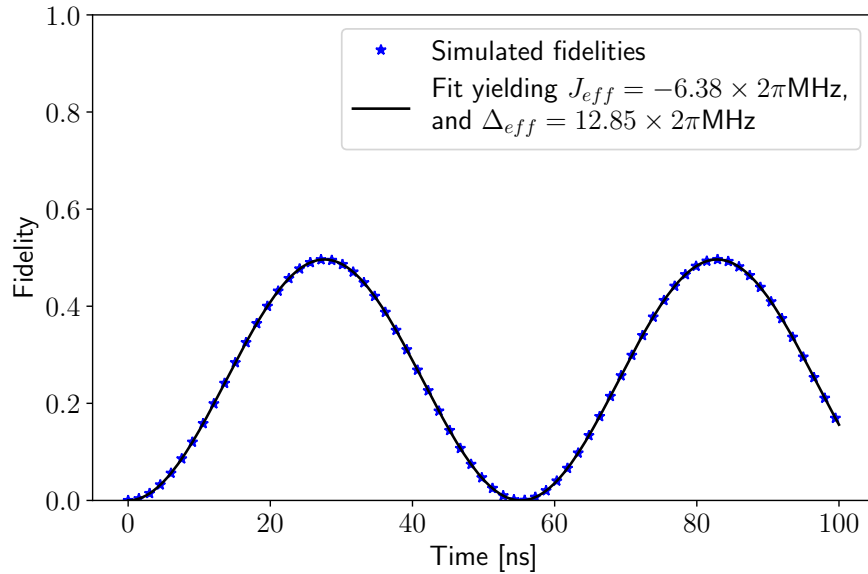


Figure 2.

with respect to the  $\sigma_0^+ \sigma_g^+ \sigma_1^- + \text{H.c.}$  interaction. The effective coupling strength we are looking for is the strength of this interaction. To find these we simply simulate the dynamics of the circuit Hamiltonian truncated to four levels in each mode and initialized in  $|1_0 1_g 0_1\rangle$  (which is also a valid state, when each mode has four states). We then calculate the fidelity with the state  $|0_0 0_g 1_1\rangle$  at subsequent times. Ideally, these two levels behave as if they are only coupled to each other, and as such follow the evolution of a single two level system, with a certain detuning and coupling between the states, described by

$$H_2 = -\frac{1}{2}\omega\sigma^z + J\sigma^x = \begin{pmatrix} -\frac{1}{2}\omega & J \\ J & \frac{1}{2}\omega \end{pmatrix} \quad (1)$$

Initializing in one of the two states described by this Hamiltonian, the evolution of the fidelity,  $F(t)$ , of the other is then described by

$$F(t) = \frac{J^2}{\omega^2/4 + J^2} \sin^2 \left( \sqrt{\frac{\omega^2}{4} + J^2} t \right). \quad (2)$$

Hence, fitting the simulated data with a sine curve gives us information about  $\Delta_{\text{eff}}$  between  $|1_0 1_g 0_1\rangle$  and  $|0_0 0_g 1_1\rangle$ , and also the effective strength,  $J_{\text{eff}}$ , of the coupling between these states. Fig. 2 shows an example of such a fit yielding the effective parameters we discussed in the main text. Clearly the fidelity does follow a sine, as if these two states are all alone in the world. This is effectively the case because all other interactions are suppressed by detuning, but as explained it is virtual processes resulting from these suppressed interactions that renormalizes the detuning and interaction strength such that we can not directly use the bare expressions found above. The bare expressions are off by a significant amount because of this renormalization as can be seen in the example below, Fig. 3. Using the described method here to find the effective parameters, however, makes it just as easy to optimize with respect to the effective parameters as the bare, though of course it takes more computation time.

### C. Optimizing circuit parameters and calculating

Higher order contributions from interactions with states outside the spin- $\frac{1}{2}$  subspace mean that we must consider effective spin model parameters when optimizing the circuit parameters. We are in particular interested in the detuning between  $|1_0 1_g 0_1\rangle$  and  $|0_0 0_g 1_1\rangle$ , and the coupling strength of the XXX-coupling. Furthermore, we want the numerical value of the anharmonicities of the modes to be about  $100 \times 2\pi\text{MHz}$  or larger in order to be able to address



the spins for initialization and control [2]. The effective detuning,  $\Delta_{\text{eff}}$ , and the effective coupling strength,  $J_{\text{eff}}$ , are found as described in the previous section.

We want to show that our circuit can be used to realize the quench dynamics presented in the main text. In this case, the effective detuning should not be zero, but rather it defines the staggered mass  $m$ . Considering the rotated Hamiltonian  $H_R$  in Eq. (3) of the main text, it can be seen that we will have  $m = \Delta_{\text{eff}}/2$ , as the energy difference between the states  $|1_0 1_g 0_1\rangle$  and  $|0_0 0_g 1_1\rangle$  is that of two particles, i.e. twice the mass,  $2m = \Delta_{\text{eff}}$ , consistent with  $\Delta_{\text{eff}}$  being the energy gap between the two states. Likewise, if  $J$  is the desired strength of the matter-gauge coupling in Eq. (1) of the main text, then  $J = 2J_{\text{eff}}$ , because of the factor  $1/2$  in the interaction term in Eq. (1). We will thus be tuning  $J/m = 4J_{\text{eff}}/\Delta_{\text{eff}}$  to find good circuit parameters producing spin model parameters that would be interesting for the analog simulation of the dynamics we found in the main text. The anharmonicities are obtained with the bare expressions given above. These too will be renormalized to some extent, but since we do not need them to have some specific value, they should simply be large, it is sufficient to calculate their bare value.

Since only the Josephson energies of a SQC can be tuned *in situ*, it is difficult to actually perform the appropriate quench of the circuit. Instead we intend for the circuit to be constructed with the post-quench parameters. The quench will then be implemented by initializing the system in the ground state of the pre-quench Hamiltonian. Whether we have the system in its pre-quench setup, go into its ground state, and then quench to the post-setup, or simply start with the system in the post-quench setup, and then quickly initialize in the ground state of the pre-quench Hamiltonian, we will see the same resulting dynamics. This moves the difficulty from performing a fast quench to performing a fast initialization. With this in mind we tune the circuit parameters to yield a negative  $J/m$  (as the quench is to a negative mass,  $m \rightarrow -m$ ), corresponding to post-quench parameters.

In Fig. 3a,b we show a set of circuit parameters, which yield  $J/m = -2.0$  and good anharmonicities. In the parameter optimization we have fixed the capacitance to ground at  $K = 1$  fF. As mentioned in the main text,  $K$  would ideally be zero, which is why we fixed it at this low value, but an experimental realization where it is completely negligible would be even better.  $E_s$ , which controls the strength of  $J_{0g1}^x$ , and thus  $J_{\text{eff}}$ , is likewise fixed at the small value of  $E_s = 0.5 \times 2\pi\text{GHz}$  to ensure that odd interactions with higher levels are suppressed by the anharmonicities. That is, the higher level interactions caused by the triple sine term, which would move population outside of the spin-1/2 subspace are suppressed by the anharmonicities, as usual. The other Josephson energies have large values, but there are also good sets of circuit parameters where they are smaller, but at the cost of  $E_s$  also being smaller, or interactions with higher levels being less suppressed. In Fig. 3c the resulting bare spin model parameters can be seen. Notice that some of the parameters are negative, despite being plotted with bars pointing in the positive direction. The bars should be used as graphical comparison of absolute sizes, while the numbers indicate the exact values. Clearly the Z-type coupling strengths are much smaller than the spin transition frequencies, which is needed as explained in the main text. In Fig. 3d the effective detuning and XXX-coupling strength, and the anharmonicities can be seen. We see that  $J_{\text{eff}}$  is noticeably smaller than the bare  $J_{0g1}^x$ . Furthermore, it is much smaller than the anharmonicities, as required to make the dynamics remain in the spin-1/2 subspace. This effective detuning and XXX-coupling strength result in  $J/m = 4J_{\text{eff}}/\Delta_{\text{eff}} = -2.0$  (corresponding to *pre-quench*  $J/m = 2.0$ ) which according to Fig. 4 of the main text would result in interesting dynamics of the order parameter and Loschmidt amplitude within a time of  $tm = 2$ , corresponding to  $t = 49.5$  ns.

In our work with tuning the circuit we have found that it is well capable of implementing the interval of  $J/m$  considered in the main text. The tuning effectively takes place via two options. Either  $J_{\text{eff}} = J/2$  is tuned separately by changing  $E_s$ , or  $\Delta_{\text{eff}} = 2m$  is tuned by changing all parameters but  $E_s$  (which does also change  $J_{\text{eff}}$ , but only slightly). While tuning  $J_{\text{eff}}$  is easy because it is proportional to  $E_s$ ,  $\Delta_{\text{eff}}$  is quite sensitive to the circuit parameters. This is essentially because in the parameter regime we are interested in,  $\Delta_{\text{eff}}$  is about the same size as  $J_{\text{eff}}$ , which itself has to be much smaller than the anharmonicities, say a factor of 10, and finally the anharmonicities are about 1 – 2% of the spin transition frequencies. Hence, the effective detuning  $\Delta_{\text{eff}}$  of the spins must be about 0.1 – 0.2% of the spin frequencies. They must therefore be tuned carefully. If a circuit is made that implements an interesting value of  $J/m$ , other nearby values could be achieved by varying just the Josephson energies, making it possible to use the same circuit to study different values of  $J/m$ .

#### D. Time evolution in rotating frame

To find an expression for the time evolution operator in a rotating frame, we essentially just have to take advantage of the fact that we can transform between the non-rotating and the rotating frame at any time using the same time-dependent operator. Imagine some state in the non-rotating frame  $|\psi(t)\rangle = U(t)|\psi(0)\rangle$ , where  $U(t)$  is the time evolution operator in the non-rotating frame. We then define a unitary, time-dependent operator  $R(t)$ , which we use to define the state in the rotating frame  $|\psi(t)\rangle_R = R(t)|\psi(t)\rangle$ , and which satisfies that the two frames are identical at  $t = 0$ , i.e.  $R(0) = \mathbb{I}$ . Let  $U_R(t)$  be the time evolution operator of the rotating frame that we seek. We then quite

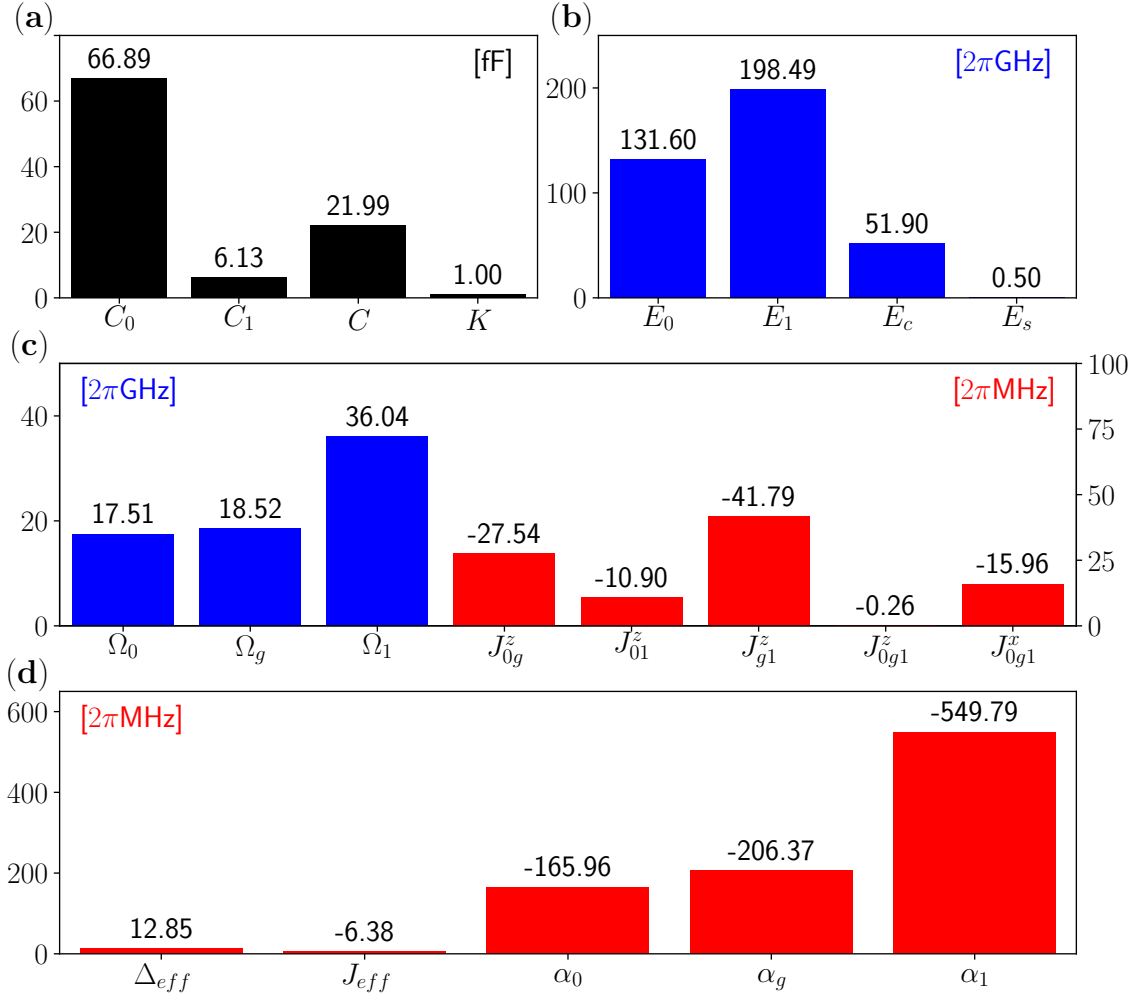


Figure 3. Circuit and spin model parameters. Notice that some parameters are negative, despite being plotted with positive bars. The bars are for graphical comparison of sizes, while the numbers above the bars give the exact value. (a),(b) Optimized circuit parameters implementing  $J/m = -2.0$  and good anharmonicities.  $K$  has been fixed at  $1\text{ fF}$  as we want it to be as low as possible.  $E_s$  has been fixed at  $0.5 \times 2\pi\text{GHz}$  to ensure that the higher level odd interactions of the triple sine-term are weak enough to be suppressed by the anharmonicities. (c) The resulting bare spin model parameters. The Z-type coupling strengths are much smaller than the spin transition frequencies as required. (d) The effective detuning and XXX-coupling strength, as well as the anharmonicities. The anharmonicities are much larger than the effective XXX-coupling strength as required, and we can see that  $J/m = 4J_{\text{eff}}/\Delta_{\text{eff}} = -2.0$ .

simply have

$$U_R(t)|\psi(0)\rangle = U_R(t)|\psi(0)\rangle_R = |\psi(t)\rangle_R = R(t)|\psi(t)\rangle = R(t)U(t)|\psi(0)\rangle$$

From this we conclude that  $U_R(t) = R(t)U(t)$ . Hence, if for example we have a Hamiltonian  $H = H_0 + H_{\text{int}}$  in the non-rotating frame, i.e.  $U(t) = e^{-iHt}$ , and we want to look at the frame rotating with respect to  $H_0$ , i.e.  $R(t) = e^{iH_0t}$ , then the time evolution operator in the rotating frame is  $U_R(t) = e^{iH_0t}e^{-iHt}$ . This is the result we used in the previous section.

### E. Calculating the average fidelity

After finding appropriate circuit parameters we do a check of the overall behaviour of the circuit, ensuring that it works as intended, including no disturbing interactions with higher levels. To do this we use average fidelity [3].

Average fidelity is a measure of how well a certain process implements a desired operation. In our case the process is the time evolution of the circuit, determined by  $H_c$  in Eq. (6) of the main text, in a frame rotating such that the resulting Hamiltonian is  $H_R$  in Eq. (3), where  $m = \Delta_{\text{eff}}/2$  and the coupling strength is  $J_{\text{eff}}$  (rather than the bare  $J_{0g1}^x$ ), as explained. To take contributions from higher level interactions into account we again truncate to the lowest *four* levels. We only rotate the spin-1/2 states, i.e. we use a four-level version of  $H_0 + \frac{1}{2}m(\sigma_0 - \sigma_1)$ , where all entries pertaining to levels higher than the spin-1/2 states are just zero. The operation we compare this with is the time evolution according to the target Hamiltonian, i.e.  $H$  from Eq. (1) of the main text with two matter sites and the gauge link between them. We compare only the dynamics of the spin-1/2 states, i.e. time evolution of the circuit takes place with four levels included for each mode, and the result is then projected down to the spin-1/2 subspace, before comparing with the time evolution of  $H$ . The average fidelity will thus be comparing the very time evolution operators themselves for the circuit and the target system. The mass and coupling strength of the target Hamiltonian are chosen to be  $\Delta_{\text{eff}}/2$  and  $2J_{\text{eff}}$ . The fidelity would thus *a priori* be expected to be quite high, but since this is all done with four levels included in each anharmonic mode, the fidelity will be a measure of how much the higher levels affect the dynamics of the circuit beyond just the renormalization of the mass and coupling strength. In particular, some population will be lost to the higher levels, and just as virtual processes contribute to the strength of the XXX-coupling, they will also to some extent induce other effective interactions. These will disturb the desired dynamics and might be gauge-variant, resulting in population moving outside of the chosen gauge sector of the spin-1/2 subspace.

The average fidelity can be calculated from [3]

$$\overline{F}(U, \mathcal{E}) = \frac{\sum_j \text{Tr} \left( U U_j^\dagger U^\dagger \mathcal{E}(U_j) \right) + d^2}{d^2(d+1)} \quad (3)$$

where  $U$  is the target operation, and  $\mathcal{E}$  is a quantum map representing the process used to implement the target operation. The  $U_j$  are a unitary basis for operators on the relevant space of states, which has dimension  $d$ . In our case the target operation is time evolution  $U = e^{-iHt}$ , with  $H = H(\Delta_{\text{eff}}/2, 2J_{\text{eff}})$  from Eq. (1). This is an operator on the spin-1/2 subspace, and so the  $U_j$  are a unitary basis for operators on that subspace. The quantum map  $\mathcal{E}$  takes an operator  $\rho$  pertaining to the spin-1/2 subspace, and returns  $\mathcal{E}(\rho) = P e^{iH_{0,\text{eff}}t} e^{-iH_c t} P^\dagger \rho P e^{iH_c t} e^{-iH_{0,\text{eff}}t} P^\dagger$ , where  $P$  is the projection operator from the four-level subspace to the spin-1/2 subspace. Hence, this map first projects the operator  $\rho$  into the four-level space, performs time evolution according to the four-level version of the circuit Hamiltonian  $H_c$ , and then projects the result back into the spin-1/2 subspace. Here  $H_{0,\text{eff}}$  is an effective four-level equivalent of  $H_0$ , taking energy shifts caused by virtual processes into account. The construction  $e^{iH_{0,\text{eff}}t} e^{-iH_c t}$  implements time evolution according to  $H_c$  in the frame rotating with respect to  $H_{0,\text{eff}}$  by first time evolving forwards with  $H_c$  and then backwards with  $H_{0,\text{eff}}$ . See the next section for details on this. We determine  $H_{0,\text{eff}}$  numerically by turning off the XXX-coupling and time evolving each of the eight spin-1/2 states in a frame rotating with respect to  $H_0$  (expanded to the four-level Hilbert space). As the Hamiltonian only involves Z-type interactions, and other, very suppressed interactions caused by the virtual processes, the spin-1/2 states will almost be eigenstates of the system, and their phase will thus be  $e^{-iE_{\text{eff}}t}$ , where  $E_{\text{eff}}$  is their effective energy. With these  $H_{0,\text{eff}}$  can be constructed.

- 
- [1] S. P. Pedersen, K. S. Christensen, and N. T. Zinner, [Physical Review Research \*\*1\*\*, 033123 \(2019\)](#).
  - [2] P. Krantz, M. Kjaergaard, F. Yan, T. P. Orlando, S. Gustavsson, and W. D. Oliver, [“A Quantum Engineer’s Guide to Superconducting Qubits,”](#) (2019), [arXiv:1904.06560](#).
  - [3] M. A. Nielsen, [Physics Letters A \*\*303\*\*, 249 \(2002\)](#).